through the remodeling of the structure and epigenetic marking of chromatin and by contacting the basal transcriptional machinery (12). PPAR activity can be pharmacologically modulated to treat major metabolic disorders (13). Thiazolidinediones are PPARγ activating drugs clinically used as insulin sensitizers but PPARγ-targeted therapeutics suffer from important adverse effects (7). The hope of better pharmaceutical strategies arises from the identification of selective PPARγ modulators (SPPARγMs) capable of uncoupling the beneficial actions of current PPARγ agonists from their side effects (13, 14).

The large PPAR ligand binding pocket, which can accommodate a wide variety of ligands, raises the question of whether PPAR activity and PPAR-regulated pathways could be affected by exposure to endocrine disrupting chemicals. Actually, PPARα was discovered as the receptor mediating hepatic peroxisome proliferation and carcinogenesis in rodents in response to a wide class of chemicals that include pesticides, industrial solvents, and plasticizers (15, 16). We have focused the present study on the interference of phthalate esters with PPAR-regulated processes. Phthalates are widely used industrial chemicals that primarily serve as plasticizers to soften PVC but are also found in cosmetics, perfumes, and certain drugs as well as in industrial paints and solvents. Diethyl-hexyl-phthalate (DEHP) is among the most abundantly used phthalate esters with an annual worldwide production estimated around 2 million tons according to Swiss authorities (Federal Office of Public Health, www.bag.admin.ch/themen/chemikalien/00228/01378). DEHP is incorporated non-covalently into flexible plastics used for manufacturing a wide variety of daily products including medical devices and food packaging and its propensity to leach can expose humans to high concentrations of this compound (17). The biological effects of DEHP are hence of major concern but so far elusive. Upon ingestion, pancreatic lipases present in the intestine convert DEHP to its monoester equivalent monoethyl-hexyl-phthalate (MEHP), which is preferentially absorbed (18). In addition, MEHP can also be produced by plasmatic and hepatic lipases, which transform DEHP directly reaching the blood through absorption or medical contamination. This metabolite activates the three PPAR isotypes and mediates the action of DEHP on hepatic peroxisome proliferation via PPARα (19–21).

This study, aimed at going beyond the toxicology approach, focuses on the molecular mechanisms through which MEHP modulates PPARγ signaling. For that purpose, we use a combination of molecular and cellular assays to directly monitor the action of the receptor in living cells. We demonstrate that MEHP promotes PPARγ-dependent adipogenesis, albeit to a lower extent than the full agonist rosiglitazone. MEHP induces the expression of a subset of PPARγ target genes required for adipogenesis when compared with rosiglitazone. Interestingly, the binding modes of MEHP and rosiglitazone to the ligand binding pocket of PPARγ seem similar. However, MEHP selectively modulates PPARγ activity according to the promoter context by promoting differential interactions with coregulators. Thus, in addition to understanding the molecular actions of MEHP beyond the toxicological observations, the combination of microscopy techniques and chromatin immunoprecipitation provides a strong molecular basis in living cells for the concept of selective PPARγ modulation.

EXPERIMENTAL PROCEDURES

Plasmid Constructs—Mouse PPARs were expressed from pSG5 vectors (reporter assay) or from pEYFP-N1 or -C1 (imaging experiments) (8). The constructs for GST-p300$_{2-516}$ (22), GST-hSRC-1$_{617-1259}$, and GST-mNCoR$_{2204-2453}$ (23) were previously described. GST-hMed1 and GST-mPGC1α were constructed by cloning PCR fragments corresponding to amino acid residues 550–716 and 1–442, respectively, in pGEX 5X3 (Amersham Biosciences). The plasmid encoding EYFP-p300$_{N\text{-}term}$ was constructed by cloning bases 1–1790 (residues 1–595) of the human p300 cDNA into pEYFP-C1 using HindIII and BamHI as restriction sites. The EYFP-Med1 receptor interacting domain construct was generated by cloning a PCR amplification product corresponding to residues 550–716 of Med1 into pEYFP-C1, using BglII and SalI. The YFP-NCoR construct was generated by cloning a PCR fragment corresponding to residues 2235–2301 of mNCoR into pEYFP-N1 using XhoI and SacII restriction sites.

Cell Culture and Transient Transfection Assays—COS7, C2C12, HeLa, and 3T3L1 cells from ATCC were maintained in Dulbecco's modified Eagle's medium supplemented with 10% fetal calf serum (Invitrogen). Transient transfection assays were performed using Lipofectamine 2000 (Invitrogen) according to the manufacturer's instructions. After transfection, cells were let to recover in medium supplemented with 10% fetal calf serum for 5 h and then grown in serum-free medium for 18 h in the presence of ligand or vehicle only. Unless otherwise stated, Wy14,643 (Cayman Chemical Co.), L-165041 (synthesized at custom in the laboratory), rosiglitazone (Sigma), MEHP (ICI), and GW9662 (synthesized at custom by Zydus Research Center, India) were used at respective final concentrations of 10^{-5}, 5×10^{-6}, 10^{-6}, 10^{-4}, and 2×10^{-5} M.

Reporter Assay—PPAR activity was monitored on a $(PPRE)_3$-luciferase reporter construct kindly provided by Dr. Evans (Salk Institute, San Diego, CA). Luciferase activity assays were performed with the Promega dual-reporter kit, according to the manufacturer's instructions. *Renilla* luciferase encoded by the normalization vector phRLTK (Promega) was used as an internal control for firefly luciferase normalization.

Adipocyte Differentiation—Two-day post-confluent 3T3L1 pre-adipocytes were induced to differentiate using two different protocols: a 10-day treatment with 10 μg/ml insulin and PPARγ ligands (rosiglitazone or MEHP) or a 2-day treatment with a differentiation mixture (10 μg/ml insulin, 1 μM dexamethasone, 0.5 mM isobutylmethylxanthine) followed by an 8-day treatment with 10 μg/ml insulin only. In both cases, the medium was changed every 48 h. After differentiation, cells were stained with Oil Red O for morphological analyses or RNA was extracted using phenol/chloroform (TRIzol, Invitrogen) and purified with Qiagen columns. For RNA extractions, four independent cultures were performed per condition. To determine triglyceride content, 3T3L1 cultures differentiated as described above in a 10-cm plate were lysed in 1500 μl of phosphate-buffered saline, 0.1% Nonidet P-40 with a Dounce

homogenizer and cytoplasmic extracts were collected. Relative triglyceride levels were evaluated by adding 100 μl of cytoplasmic extract to 200 μl of Infinity triglyceride reagent (Thermo-Electron Corporation) and measuring the absorbance at 500 nm. The levels of triglyceride were normalized to protein levels measured with the Bradford reagent (Bio-Rad) at 595 nm.

siRNA Knockdown—An oligonucleotide (5′-GATCCCCAAAGCCAAGGCGAGGGCGATCTTTTCAAGAGAAAGATCGCCCTCGCCTTGGCTTTTTTTTGGAAA-3′) encoding a PPARγ siRNA (5′-AAAGCCAAGGCGAGGGCGATCTT-3′) as a hairpin was cloned into the pLVTH lentiviral vector as previously described (24). Viral production was performed according to Ref. 24 and 3T3L1 cells were infected at a multiplicity of infection of 10.

Quantitative Reverse Transcription-PCR—Reverse transcription was performed with random hexamers on 1 μg of total RNA using the SuperScript first-strand synthesis system (Invitrogen) and the reaction was diluted 100 times for amplification. PCR were performed in triplicate in 384-well plates on an Applied Biosystems 7900HT cycler using commercial Taq-Man probes (Applied Biosystems). Results were normalized to 3 housekeeping genes (TATA-box binding protein, eukaryotic translation elongation factor α1, and ribosomal protein S9) and quantified using qBase (25).

Microarray Experiments—The mouse cDNA microarrays used in this study consisted of roughly 17,000 PCR products generated from cDNA clones and control DNAs spotted onto Nexterion AL slides (Schott). A complete description of the slides and their content can be obtained from the Lausanne DNA Array Facility (www.unil.ch/dafl). RNA quality was assessed using the RNA 6000 Nanochip assay (Agilent Technologies). A single round of amplification was performed with 3 μg of total RNA using the MessageAmp aRNA Amplification Kit (Ambion) following the protocol provided. 5 μg of amplified RNA was reverse transcribed with SuperScript II reverse transcriptase (Invitrogen) and random hexamers for 2 h at 42 °C, in the presence of either Cy3-dCTP or Cy5-dCTP (GE Healthcare). RNA was hydrolyzed by heating at 65 °C for 15 min in a basic environment. The solution was then neutralized and labeled cDNA was purified using a Qiagen MiniElute PCR Purification kit. The Cy3- and Cy5-labeled targets were combined, mixed with Cot 1 DNA (Invitrogen), polyadenylic acid (Sigma), and yeast tRNA (Sigma), and hybridized on custom glass microarrays at 64 °C for 20 h in 3× SSC, 0.4% SDS. Slides were then washed twice for 5 min in 2× SSC, 0.1% SDS, twice for 1 min in 0.2× SSC, once for 1 min in 0.1× SSC, and once for 5 min in 0.1× SSC, 0.1% Triton X-100. After drying, slides were scanned on a microarray scanner (Agilent Technologies) and the resulting TIFF images were analyzed using the GenePix Pro 6.0 software (Molecular Devices).

Statistical analysis was performed with the R software packages sma (26) and limma (27). Gene expression was quantified with the sma package using print tip group lowess normalization without background subtraction (26, 28). The three treatments (V, rosiglitazone, and MEHP) were compared pairwise using a linear model. Differential expression was assessed by fitting the linear model for the effects of the two treatments considered and computing moderated *t* statistics and Benjamini and Hochberg false discovery rates with the limma package (27, 29).

Pulldown Experiments—GST fusion proteins were expressed in *Escherichia coli* and purified on a glutathione affinity matrix (GE Healthcare). mPPARγ was produced *in vitro* with reticulocyte lysates (Promega) and labeled with [^{35}S]methionine. 3 μg of GST fusion proteins were then incubated with 15 μl of programmed reticulocyte lysate in 500 μl of binding buffer (Tris-HCl, pH 7.4, 25 mM; EDTA 1 mM; NaCl 100 mM; Triton X-100 0.1%; phenylmethylsulfonyl fluoride 0.2 mM; protease inhibitor mixture (Roche)) supplemented with 0.5% dry milk, during 4 h at 4 °C, with Me_2SO, 10 μM rosiglitazone, or 1000 μM MEHP. Beads were washed 3 times with binding buffer and samples were boiled with 40 μl of 2× SDS-PAGE buffer (12,5 mM Tris-HCl, 20% glycerol, 0.002% bromphenol blue, 5% β-mercaptoethanol), separated on a 10% SDS-PAGE gel, transferred onto a nitrocellulose membrane and exposed to a PhosphorImager (Typhoon, Amersham Biosciences).

Chromatin Immunoprecipitation Experiments—After 10 days of treatment, cells were washed twice in phosphate-buffered saline and cross-linked for 10 min at room temperature in 1% formaldehyde. Cross-linking was stopped by a 5-min incubation in 0.125 M glycine and chromatin was subsequently extracted as previously described (30). Chromatin resuspended in 500 μl/10-cm cell culture dish was then sonicated on ice with a 24-channel multisonicator (Sonics Vibra cell) set at 40% during 120 s in 5-s sonication periods spaced by 10 s. After centrifugation, sonicated supernatants from 10 independent cultures performed were pooled in a final volume of 5 ml and immunoprecipitations were performed in triplicate with 250 μl of sonicated lysate diluted 2.5-fold in IP buffer (2 mM EDTA, 100 mM NaCl, 20 mM Tris-HCl, pH 8.1, and 0.5% Triton X-100) after a 3-h preclearing at 4 °C with 5 μg of sheared salmon sperm DNA, and 150 μl of a 50% protein A-Sepharose bead (Amersham Biosciences) slurry. Immunoprecipitations were performed overnight at 4 °C under rocking with 0.5 μg of anti-Pol II antibody (Upstate Biotechnology; Clone CTD4H8 number 05-623), 1 μg of anti-p300, anti-NCoR, and anti-PGC1 (Santa Cruz; sc-584, sc-1609, and sc-13067, respectively) and 1.5 μg of anti-hemagglutinin epitope, anti-SRC1, and anti-TRAP220 (Santa Cruz; sc-805, sc-6096, or sc-5335, respectively). Complexes were recovered after a 3-h incubation at 4 °C with 2 μg of sheared salmon sperm DNA and 50 μl of protein A-Sepharose. Precipitates were then serially washed, using 300 μl of Washing Buffers (WB), in combinations specific for each antibody: WB I (2 mM EDTA, 20 mM Tris-HCl, pH 8.1, 0.1% SDS, 1% Triton X-100, 150 mM NaCl), WB II (2 mM EDTA, 20 mM Tris-HCl, pH 8.1, 0.1% SDS, 1% Triton X-100, 500 or 250 mM NaCl), WB III (1 mM EDTA, 10 mM Tris-HCl, pH 8.1, 1% Nonidet P-40, 1% deoxycholate, 0.25 M LiCl) and then twice with 1 mM EDTA, 10 mM Tris-HCl (pH 8.1). Combinations were as follows: Pol II (WB I, WB II (500 mM NaCl), WB III); CBP (WB I, WB II (500 mM NaCl), WB III, 2 times); SRC1 (WB I, WB II (250 mM NaCl) × 2); TRAP220 (WB I, WB II (250 mM NaCl), 2 times), NCoR (WB I, WB II (250 mM NaCl), 2 times); and PGC1 (WB I, WB II (500 mM NaCl), WB III). Precipitated complexes were removed from the beads through three sequential incubations of 10 min with 50 μl of 1% SDS, 0.1 M $NaHCO_3$. Cross-linking

was reversed by an overnight incubation at 65 °C. DNA was next purified with Qiaquick columns (Qiagen) and eluted in 10 μl of H_2O. 2 μl of inputs and ChiP DNA were then assayed in real time PCRs using a Bio-Rad MyiQ apparatus and Bio-Rad iQ SYBR Green supermix and 1 μM primers (Proligo, France). Results from three independent experiments were normalized to inputs using the Δ/ΔCt method.

Fluorescence Correlation Spectroscopy (FCS) Experiments—FCS was performed on a LSM510 ConfoCor2 (Zeiss) as previously described (8). Briefly, intensity fluctuations of the fluorescence collected between 505 and 550 nm were detected using an avalanche photodiode and recorded at 5 spots in each nucleus, with a repetition of 10 measurements per spot. Using the Origin software, the autocorrelation curves were fitted to an anomalous diffusion model to derive diffusion times, which were subsequently converted to diffusion coefficients and averaged over at least 10 cells.

Fluorescence Resonance Energy Transfer (FRET) Experiments—Sensitized emission FRET was monitored at 37 °C over at least 50 living cells using a TCS SP2 AOBS confocal microscope (Leica) as previously described (9, 31). Briefly, fluorescence was recorded in three different settings: CFP_{ex}, 405 nm, CFP_{em}, 465–485 nm; YFP_{ex}, 514 nm, YFP_{em}, 525–545 nm; $FRET_{ex}$, 405 nm, $FRET_{em}$, 525–545 nm. Laser power and detector gain were adjusted in the different channels so that equimolar concentrations of CFP and YFP give equal intensities (equimolar concentrations of CFP and YFP were obtained by expressing a fusion protein of CFP and YFP spaced by 475 residues). Settings were kept unchanged for analysis of all samples. As the ratio of CFP spectral bleed-through into the FRET channel ($SBT_{CFP} = I_{FRET}/I_{CFP}$) determined on cells expressing CFP alone has been previously observed to vary with CFP intensity, this variation was modeled using an exponential fit (31). In contrast, the ratio of YFP spectral bleed-through into the FRET channel ($SBT_{YFP} = I_{FRET}/I_{YFP}$) determined on cells expressing YFP alone was a constant equal to the average ratio. FRET measured in co-expressing cells was then corrected for spectral bleed-throughs and normalized for expression levels according to the following formula (31),

$$\text{expNFRET} = \frac{I_{FRET} - I_{CFP} \times (e \times \exp(I_{CFP} \times f) + g) - I_{YFP} \times b}{\sqrt{I_{CFP} \times I_{YFP}}} \quad \text{(Eq. 1)}$$

where I_{FRET}, I_{CFP}, and I_{YFP} are the intensities measured with the FRET, CFP, and YFP settings in the presence of both the donor and acceptor, e, f, and g are the constants determined by the fitting of the CFP SBT ratio in the presence of CFP only, and b is the average YFP SBT ratio in the presence of YFP only.

Structural Modeling—Missing parameters for MEHP, for use in conjunction with the CHARMM22 (32) all atoms molecular mechanics force field, were derived from the Merck Molecular Force Field (MMFF (33)), by taking the dihedral angle term as is, but only the quadratic part of the bond and angle energy terms. The partial charges and van der Waals parameters of the ligand atoms were taken from the MMFF. The ligand was modeled with all hydrogens.

To take account of a possible induced fit of the protein upon ligand complexation, the docking of MEHP to hPPARγ was realized based on two experimental x-ray structures of the hPPARγ ligand-binding domain (LBD) in complex with two different ligands. The first corresponds to the structure of the complex with the agonist AZ242 obtained at 2.35-Å resolution (PDB code 1I7I (34) in the Protein Data Bank (35)). The second structure corresponds to the complex of hPPARγ with an α-aryloxyphenylacetic acid partial agonist obtained at 2.5-Å resolution (code 1ZEO (36) in the PDB). The two structures differ in the conformation of residues Phe^{282} (H3), Gln^{286} (H3), and Phe^{363} (loop between H6 and H7). In 1ZEO, these residues, together with residues Ile^{281} (H3), Leu^{356} (H6), Phe^{360} (loop between H6 and H7), Leu^{453} (H11), and Leu^{465} (loop between H11 and H12), form a hydrophobic pocket where the benzisoxazol group fits. This pocket is closed in the 1I7I structure due to an alternate positioning of Phe^{282}, Gln^{286}, and Phe^{363}. Both ligands of the template complexes have a carboxylate function, like MEHP. They were removed from the binding site prior to MEHP docking.

Four calculations were performed, corresponding to the docking of the *R* or *S* configurations of MEHP in the 1I7I or 1ZEO structures. The protein was held fixed in all cases, the protein flexibility being taken into account through the use of different experimental structures. The details of the calculations will be presented separately.[5] In brief, starting from a set of 250 randomly generated initial conformations, positions, and orientations of MEHP inside the known binding site of hPPARγ, the coordinates of the ligand were refined using several operators, renewing 10% of the population at each generation. The thorough exploration of the accessible conformational space of the ligand relative to the protein surface was submitted during 400 generations to the evolutionary pressure of a scoring function that takes account of the solvent effect thanks to the GB-MV2 implicit solvent model (37). The lowest energy conformation was retained as the proposed binding mode. The accessible conformational space was defined as a 15-Å radius sphere centered on the center of mass of the AZ242 ligand. This region is large enough to explore possible pauses on the protein surface, out of the binding site. Actually, it has been observed that the pauses proposed by EADock for bad ligands are situated out of the known binding site of the targeted protein (data not shown). In all models of MEHP binding to PPARγ, the energetically most favorable calculated binding mode is situated inside the known binding site of the protein, consistent with the ability of MEHP to transactivate PPARγ.

Statistical Analyses—Data are represented as average ± S.E. of the mean. Statistical significance was determined using an analysis of variance followed by Tukey's post hoc test.

RESULTS

MEHP Is a Partial PPARγ Agonist Whose Efficacy Varies According to the Cell Type—MEHP was previously reported to activate PPARs in transactivation assays (19–21). However, the levels of activation varied between studies, possibly

[5] Grosdidier, A., Zoete, V., and Michielin, O. (2007) *Proteins* **67**, 1010–1025

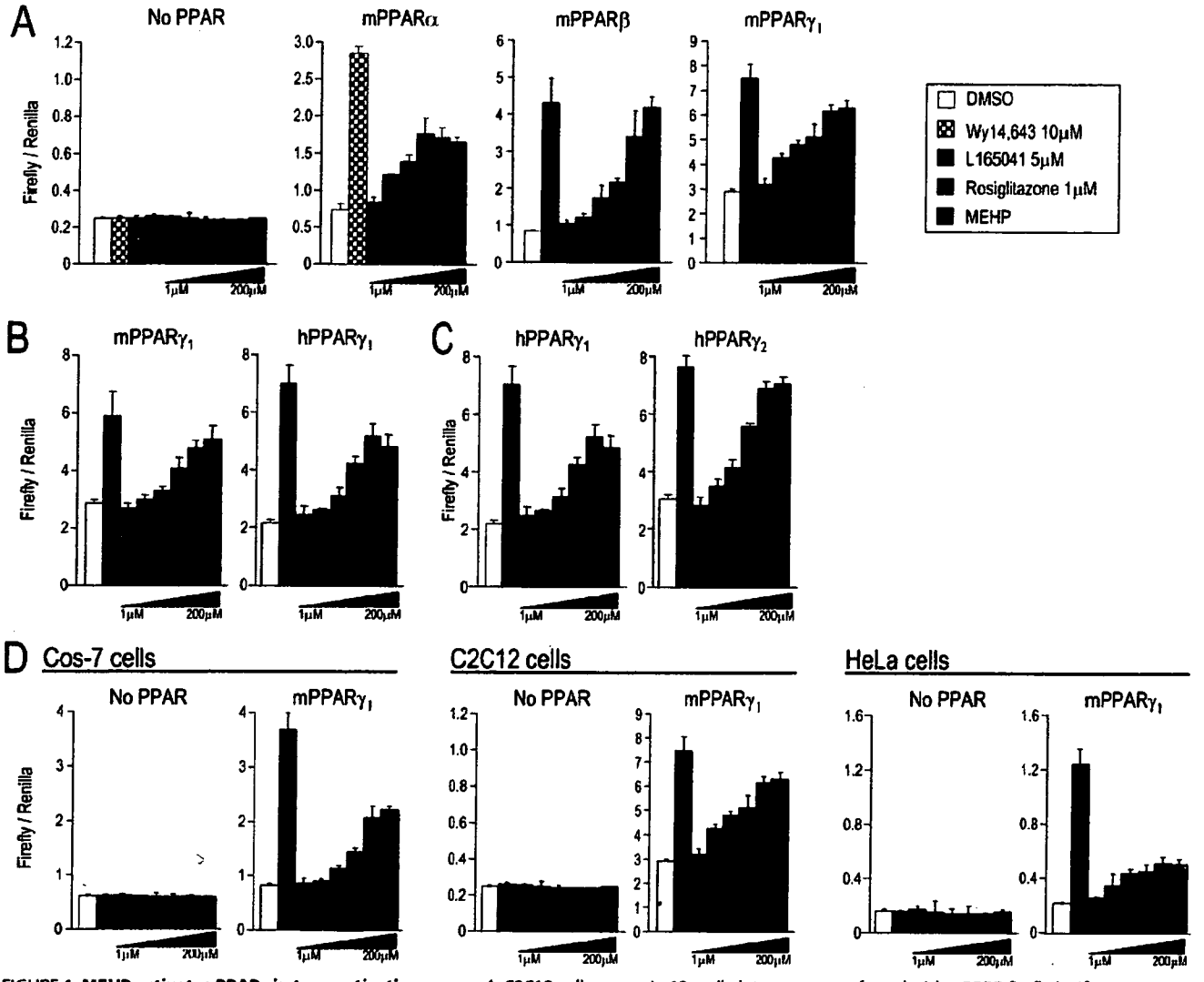

FIGURE 1. **MEHP activates PPARs in transactivation assays.** *A*, C2C12 cells grown in 12-well plates were transfected with a PPRE-firefly luciferase reporter construct (600 ng/well), a normalization vector encoding *Renilla* luciferase (5 ng/well) and an expression vector, either empty or coding for mouse PPARα, PPARβ, or PPARγ1 (250 ng/well). After transfection, cells were treated with Me_2SO (1%) or the indicated ligands for 18 h (10 μM Wy14,643, 5 μM L-165041, 1 μM rosiglitazone, and 1/3.2/10/32/100 and 200 μM MEHP). Firefly luciferase activity of 4 biological replicates was normalized to the corresponding *Renilla* luciferase activity. Similar transactivation assays were then performed as described in *A* with mouse or human PPARγ1 in C2C12 cells (*B*) and with human PPARγ1 or PPARγ2 in C2C12 cells (*C*) and with mouse PPARγ1 in different cell types (*D*).

because of the use of different cell types, different reporter systems, and receptors from different species. To characterize the action of this phthalate monoester on full-length PPARs, we assessed the ability of MEHP to induce the transcription of a reporter construct containing 3 PPREs upstream of the luciferase cDNA in the presence of the different PPAR isotypes. MEHP could activate mouse PPARα, PPARβ, and PPARγ1, albeit to a generally lower extent than the reference agonists (Fig. 1*A*). PPAR activation was detected with doses as low as 3.2 μM and reached maximum levels at 100 μM. Maximal activation of PPAR by MEHP was approximately half of that achieved with Wy14643 and rosiglitazone for PPARα and PPARγ, respectively, whereas the maximal levels of PPARβ activation achieved with MEHP and L165041 were comparable. We decided to focus this study on the activation of PPARγ by MEHP and therefore evaluated potential species and isoform differences. Both the mouse and human PPARγ1 receptors where activated with similar affinity and efficacy in C2C12 cells (Fig. 1*B*). The additional 30 N-terminal residues of the PPARγ2 isoform only mildly affected the ability of MEHP to activate the receptor by slightly increasing the maximal level of activation without affecting affinity (Fig. 1*C*). Surprisingly, the ability of MEHP to activate PPARγ was cell-type dependent (Fig. 1*D*). Whereas the affinity of the compound for PPARγ was comparable in the three cell lines tested (EC_{50} around 30 μM), the efficacy of MEHP relative to the reference agonist clearly differed between cell lines, the high dose reaching 80% of the rosiglitazone activation level in C2C12 cells, but only 60% in COS7 cells and 35% in HeLa cells. Altogether, these experiments demonstrate that MEHP is a partial pan-PPAR agonist with reduced affinity and efficacy compared with full agonists.

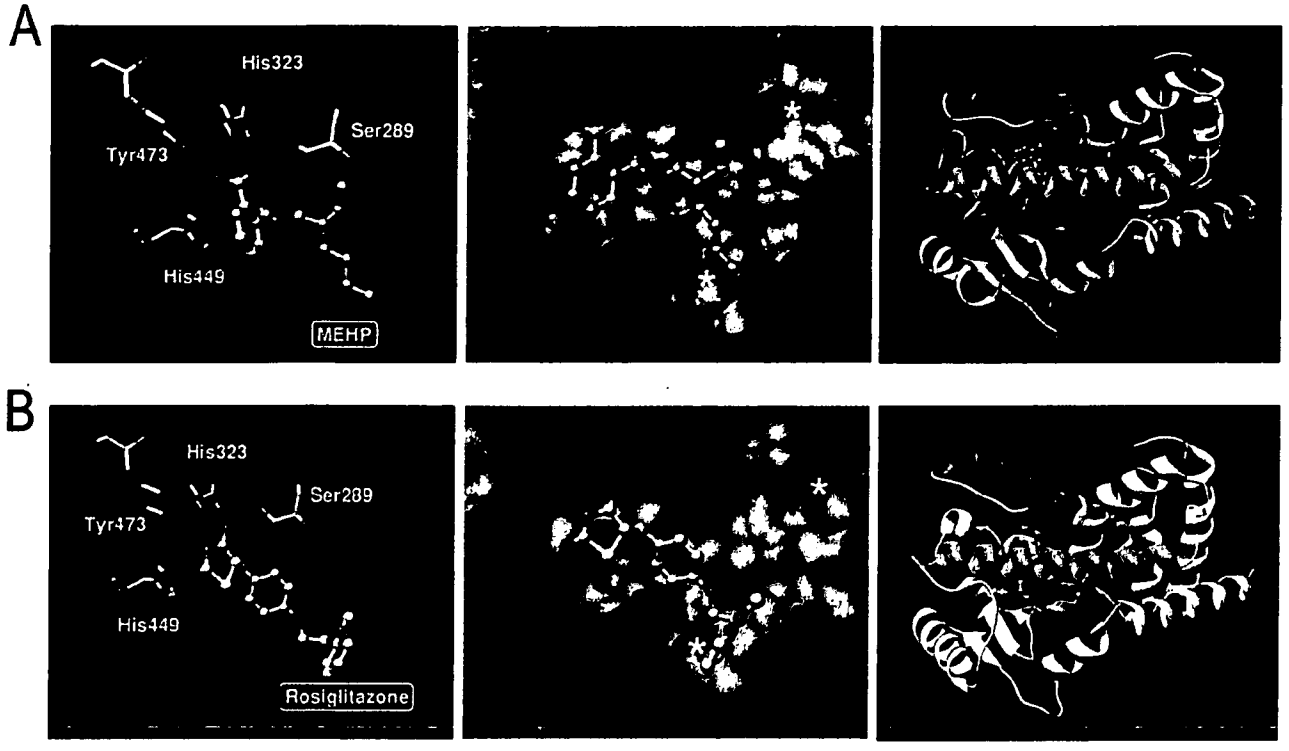

FIGURE 2. **MEHP and rosiglitazone bind similarly to the PPARγ ligand-binding domain.** The binding of the *R* enantiomer of MEHP to the human PPARγ LBD (structure 1I7I) was modeled as described under "Experimental Procedures" (*A*) and compared with the reported structure of the hPPARγ LBD complex with rosiglitazone (*B*). *Left panels* represent interactions with key residues of the LBD. *Middle panels* describe the positioning in the LBD cavity where *asterisks* represent the two parts of the T-shaped ligand binding pocket. The *right panels* show the position of the ligand in the secondary structure of the receptor. Helixes contacting the ligand are colored as follows: H3, *green*; H5, *orange*; H11, *red*; and H12, *blue*. Hydrogen atoms were included in the modeling of the binding mode of MEHP but these atoms were removed from the representation for clarity because rosiglitazone hydrogens are not present in the structure from the data base.

To characterize whether differences in binding mode could potentially account for the differences in PPARγ activation by MEHP and rosiglitazone, we modeled the binding of MEHP to two reference structures (1I7I (34) and 1ZEO (36)) of the PPARγ LBD and compared it to the binding of rosiglitazone available from the crystal structure of the PPARγ LBD in complex with this agonist (38). The results obtained for the docking of MEHP in the 1I7I and 1ZEO structures of hPPARγ are very similar and both the *R*- and the *S*-enantiomer of MEHP could fit in the PPARγ LBD (data not shown). Although explored by the ligand during the docking process, the additional pocket of 1ZEO was not used in the proposed binding mode ("Experimental Procedures"). MEHP contacted Ser^{289}, His^{323}, His^{367}, and Tyr^{473} (Fig. 2*A*), a set of residues important for the stabilization of the interaction between rosiglitazone and the receptor (38) (Fig. 2*B*). Furthermore, the contact between the carboxylate function of the phtalic acid ring and Tyr^{473}, a residue from helix 12 important for transcriptional activation, suggests that the activity of MEHP relies on the stabilization of helix 12. This observation supports the absence of activity of the DEHP parent compound (39) where this carboxylate is esterified by a bulky and hydrophobic chain. MEHP and rosiglitazone bind to the PPARγ LBD in similar configurations where only one side of the T-shaped binding pocket is occupied and where similar residues are contacted. Thus, the difference in affinity and in efficacy between MEHP and rosiglitazone most likely reflect subtle variations in the binding mode that may lead to less productive conformational changes upon MEHP binding. However, the full characterization of the differential changes in the three-dimensional structure of the LBD would require the crystallization of the PPARγ LBD in complex with MEHP.

Selective Recruitment of Coregulators by MEHP—Coregulator recruitment is the major functional determinant that follows conformational changes of the nuclear receptor LBD in response to ligand binding. We thus compared how MEHP and rosiglitazone modulate interactions with corepressors and coactivators, which assist PPARγ to regulate transcription. This experiment is classically assayed *in vitro*. However, many other factors in the nucleus of the living cell may also affect protein-protein interactions. FCS is a technique measuring the diffusion of fluorescent molecules at high temporal resolution that can be used in the living cell. Using this technique, we previously showed that the YFP-PPAR mobility in cells is reduced by ligand binding (8). Because this reduction in mobility is caused by the formation of large complexes through coactivator recruitment (9), we hypothesized that a selective recruitment of coactivators in response to MEHP compared with rosiglitazone binding could potentially translate into different patterns of YFP-PPARγ mobility. We thus compared YFP-PPARγ diffusion coefficients by FCS in COS7 cells in the presence and absence of rosiglitazone and MEHP. Diffusion coefficients were indeed reduced from 8 to 6.5 $\mu m^2/s$ in

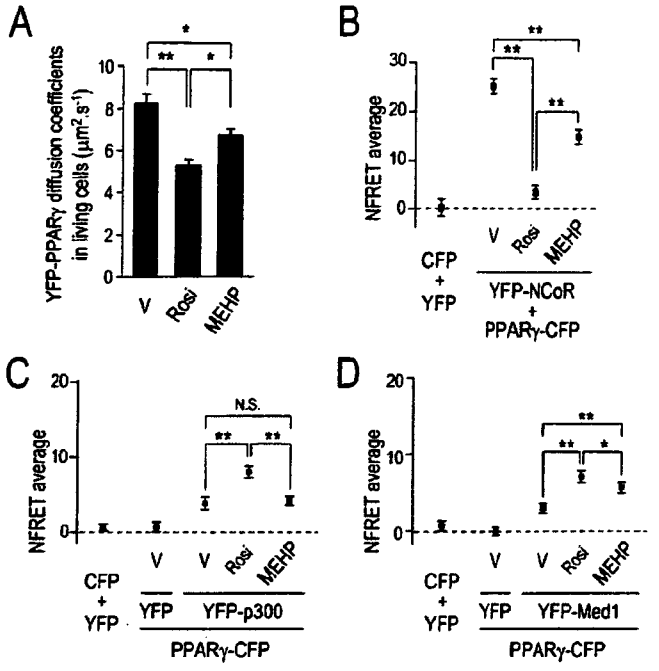

FIGURE 3. **MEHP induces selective interactions between PPARγ and coregulators in living cells.** *A*, FCS assays in living cells. The diffusion of YFP-PPARγ was measured by FCS in living COS-7 cells expressing very low levels of the fusion protein. Diffusion coefficients were calculated from diffusion times extracted by fitting autocorrelation curves to a model of anomalous diffusion. *B–D*, FRET assays in living cells. FRET was measured in living COS-7 cells expressing equimolar amounts of PPARγ-CFP and YFP-NCoR$_{2235-2301}$ (*B*), YFP-p300$_{1-595}$ (*C*), or YFP-Med1$_{550-716}$ (*D*). The concentrations of rosiglitazone and MEHP were 1 and 100 μM, respectively. * and ** indicate *p* values smaller than 0.05 and 0.01, respectively, according to an analysis of variance followed by Tukey's post hoc test.

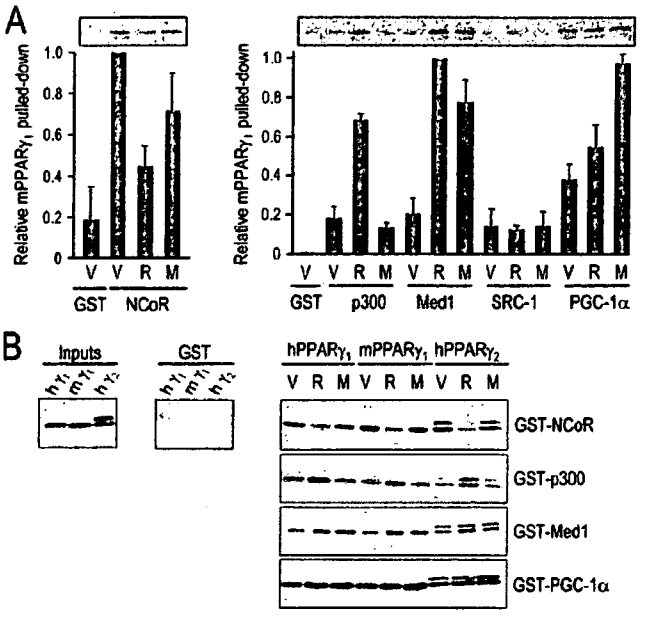

FIGURE 4. **MEHP induces selective interactions between PPARγ and coregulators *in vitro*.** *A*, the recruitment of [^{35}S]mPPARγ1 to GST-labeled corepressor or coactivators immobilized on Sepharose beads was quantified by phosphorimager in the presence of vehicle (*V*), 10 μM rosiglitazone (*R*), or 1000 μM MEHP (*M*) and values were plotted as ratios to the values for vehicle (corepressor) or Med1 + Rosi (coactivators). *B*, GST pull-downs were performed as in *A* with [^{35}S]hPPARγ1, [^{35}S]mPPARγ1, and [^{35}S]hPPARγ2 to compare species- and isoform-specific effects. The second band observed for PPARγ2 likely results from the use of the alternate PPARγ1 start codon during *in vitro* translation.

response to MEHP, whereas they were further reduced to 5 μm^2/s by rosiglitazone (Fig. 3*A*). The sizes of PPARγ-coactivator complexes formed by MEHP binding, which are directly evaluated in living cells using this assay, are therefore smaller than those formed in response to rosiglitazone and reflect different complex compositions.

To identify the regulators recruited by rosiglitazone and MEHP, we analyzed their respective ability to trigger corepressor release and coactivator recruitment. Interactions with individual coregulators were assessed in the native context of a living cell using FRET imaging. The levels of energy transfer, which reflect direct interactions, were measured in living cells co-transfected with CFP-tagged PPARγ and large coregulator domains tagged with YFP. Transfection conditions were optimized to ensure low and equimolar expression levels and the analyses were restricted to cells without aberrant localization seen upon high levels of expression (8). The strong interaction between PPARγ and NCoR observed in the absence of ligand was totally abolished in the presence of rosiglitazone but MEHP had only a partial effect on this interaction (Fig. 3*B*). Using a similar assay, a basal interaction was detected between PPARγ and p300 and the Med1 subunit of the mediator complex (also called TRAP220, DRIP205, and PBP) in the absence of ligand (Fig. 3, *C* and *D*). Rosiglitazone significantly enhanced the interaction with p300 and Med1, whereas MEHP promoted the recruitment of Med1 but was totally inefficient in inducing the recruitment of p300. MEHP therefore selectively regulates interactions with coregulators in living cells both at the levels of transcriptional complex size and interactions with individual corepressors and coactivators.

The interaction with PGC1α could not be evaluated by FRET as this construct gave no FRET signal with PPARγ, most probably because of inappropriate fluorophore spacing and orientation. We therefore confirmed our live cell results and extended them to other coregulators using an *in vitro* pull-down assay where GST-tagged coregulators were immobilized on beads and [^{35}S]mPPARγ1 recruitment was evaluated (Fig. 4*A*). In this assay, the binding of SRC-1 to PPARγ was very weak and was not influenced by ligand binding but consistent with our FRET assays, MEHP induced only a partial release of NCoR, and a strong recruitment of Med1, but not of p300. The PPARγ coactivator 1α (PGC-1α) strongly interacted with PPARγ in the absence of ligand and this interaction was modestly enhanced by rosiglitazone but strongly enhanced by MEHP. We also took advantage of this *in vitro* assay to assess species- and isoform-specific effects in coregulator recruitment in response to MEHP. The profile of coregulator recruitment to human PPARγ1 and to the PPARγ2 isoform in response to MEHP was very similar to that observed with mouse PPARγ1 (Fig. 4*B*). Altogether, these experiments demonstrate that when compared with the action of the full agonist rosiglitazone, MEHP induces a selective recruitment of PPARγ coregulators with stronger interactions with PGC-1α but a lack of p300 recruitment.

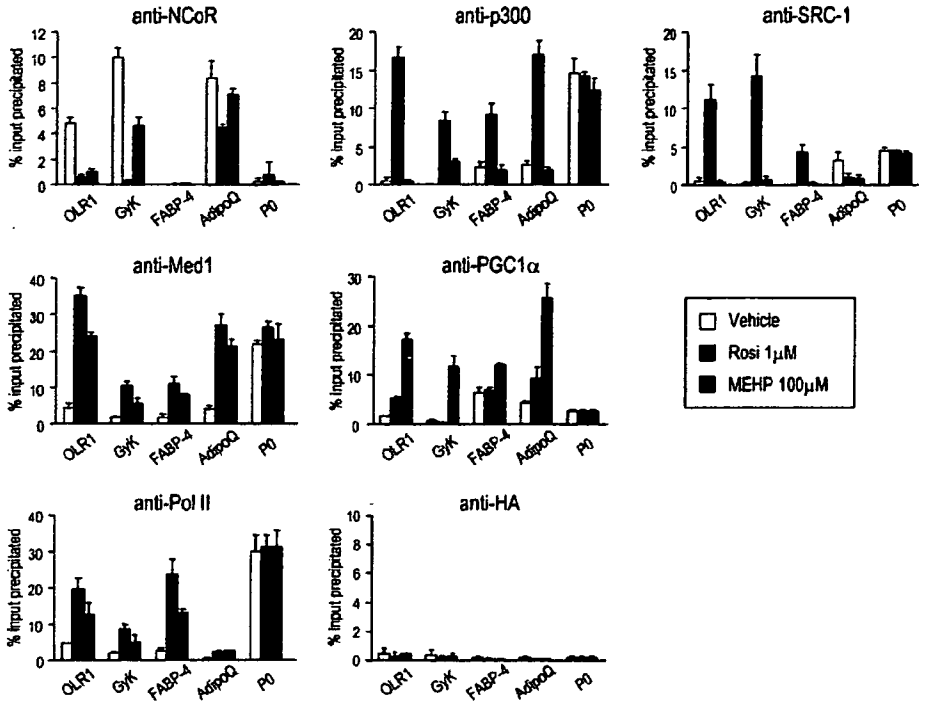

FIGURE 5. **MEHP induces the selective recruitment of coregulators on PPARγ target promoters.** 3T3L1 cells, treated for 10 days with a combination of 10 μg/ml insulin and vehicle (Me_2SO, 1%), rosiglitazone (*Rosi*), or MEHP at the indicated concentrations, were cross-linked and subjected to chromatin immunoprecipitation as described under "Experimental Procedures." The DNA fragments immunoprecipitated in three independent immunoprecipitations by specific antibodies against coregulators or a control hemagglutinin (*HA*) antibody were analyzed by quantitative reverse transcriptase-PCR.

and ligand-dependent co-regulator recruitment strikingly correlates with the interaction assays.

MEHP Promotes Adipocyte Differentiation through PPARγ—To investigate the action of MEHP on PPARγ-regulated pathways at the cellular level, we studied the influence of MEHP on adipogenesis, a well characterized PPARγ-regulated function. As expected, a 10-day treatment of 3T3L1 pre-adipocytes with the full PPARγ agonist rosiglitazone in the presence of insulin strongly induced adipogenesis in a dose-dependent manner, as evidenced by Oil Red O staining at low (Fig. 6*A*) and high magnification (Fig. 6*B*). Whereas insulin alone had only mild effects, the combination of insulin and MEHP also induced dose-dependent adipogenic effects, whereas the DEHP parent compound was inefficient in inducing adipocyte differentiation. The ability of MEHP to promote adipogenesis appeared at a dose of 10 μM and was maximal at 100 μM, with no further enhancement at higher doses (data not shown). However, the maximal effect induced by MEHP was lower than that induced by rosiglitazone. The actions of both ligands on adipocyte differentiation were confirmed by quantification of cellular triglyceride contents that were strongly induced by rosiglitazone but only partially induced by MEHP (Fig. 6*C*). Thus, although MEHP significantly induces adipocyte differentiation, this phthalate monoester has a reduced adipogenic potential compared with rosiglitazone, most likely related to the selective modulation of its activity through differential coregulator recruitment.

Selective Recruitment of Coregulators by DNA-bound PPARγ in the Presence of MEHP—FCS and FRET analyses cannot specifically assess the property of the complexes bound to DNA. We thus needed to establish whether the selective interactions in the nucleus of living cells also translate into selective recruitment of coregulators by DNA-bound PPARγ-containing complexes. Using specific antibody against each of the coregulators, we performed chromatin immunoprecipitation and assessed PPARγ target promoter occupancy, in the presence of either rosiglitazone or MEHP (Fig. 5). The promoter of the ribosomal protein P0 was used as a reference gene, not regulated by PPARγ, and precipitation with the unrelated hemagglutinin antibody served as a negative control. A control experiment using a PPARγ antibody could not be reliably realized, likely due to the poor quality of the various antibodies tested (data not shown). As previously described, in the absence of PPARγ ligand, NCoR was associated with the glycerol kinase (*Gyk*) and oxidized low density lipoprotein receptor 1 (*Olr1*) promoters, but not with the fatty acid-binding protein 4 (*Fabp-4*)/*aP2* promoter, and this association disappeared with rosiglitazone treatment (10, 40). Consistent with our FRET and pull-down observations, MEHP induced a partial clearance of NCoR from these two PPARγ target promoters. The recruitment of coactivators is also consistent with our observation in the living cells. Unlike rosiglitazone, MEHP did not promote recruitment of p300 or SRC-1 on target promoters. However, it induced a recruitment of Med1 to slightly lower levels than those achieved by rosiglitazone but a recruitment of PGC-1α at much higher levels. Thus, the global pattern of promoter-specific

To address whether the actions of MEHP on adipogenesis require PPARγ, we inhibited PPARγ either by antagonist treatment or by generating a 3T3L1 cell line stably expressing an anti-PPARγ siRNA through lentiviral infection. Treatment with an excess of the GW9662 antagonist partially but significantly inhibited the adipogenic actions of MEHP and rosiglitazone (Fig. 6*D*). Consistently, the effects of both compounds on adipocyte differentiation were significantly reduced in PPARγ siRNA cells, whereas cells infected with a virus containing the empty pLVTH vector underwent similar differentiation as WT cells (Fig. 6*E*).

MEHP Induces Selective Transcriptional Regulations during Adipocyte Differentiation—To characterize the differences in the adipogenic actions of MEHP and rosiglitazone and the underlying molecular pathways, we performed gene expression array analyses on glass slides spotted at custom with a collection of 17,000 mouse cDNAs. Expression levels from undifferentiated cells treated with insulin only and from cells differentiated with rosiglitazone or MEHP in the presence of insulin were

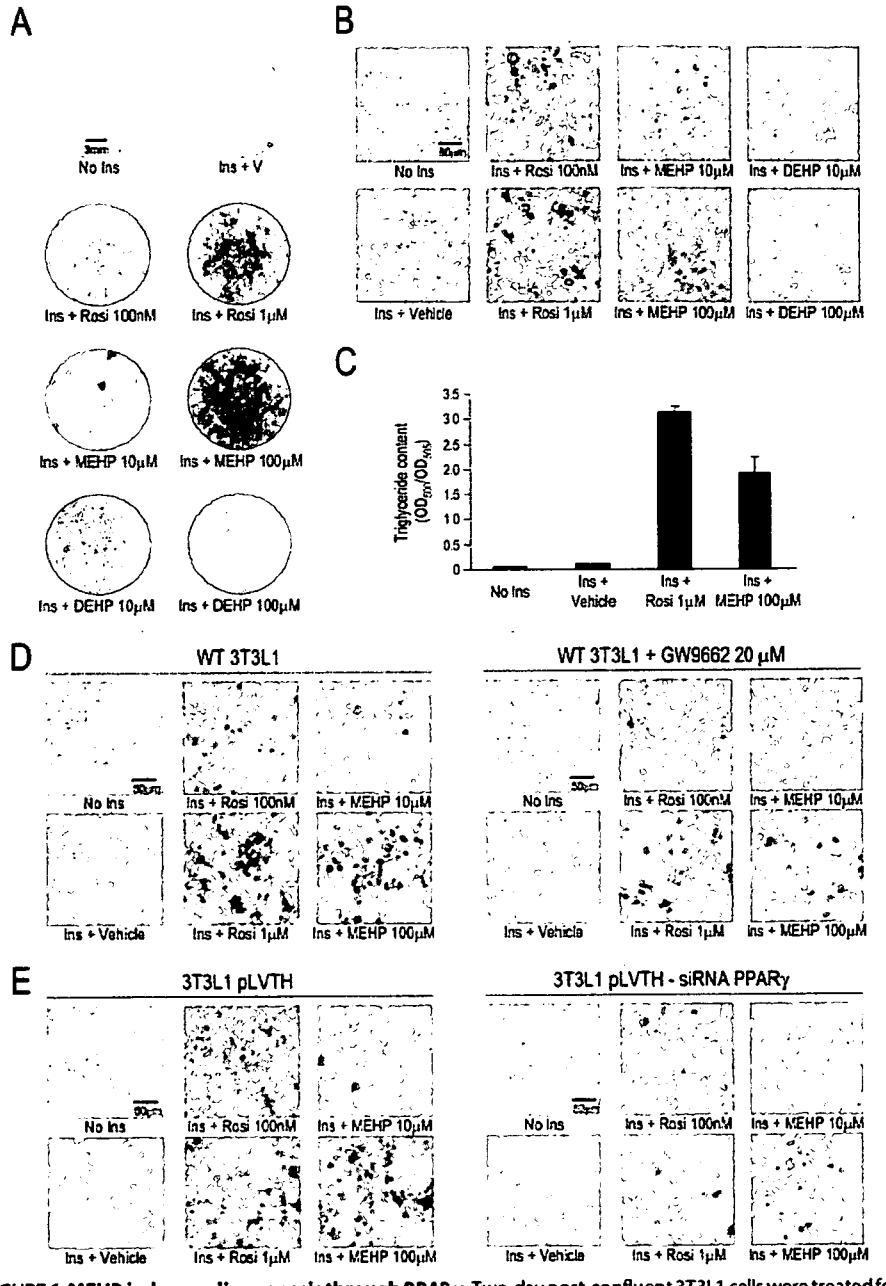

FIGURE 6. **MEHP induces adipogenesis through PPARγ.** Two-day post-confluent 3T3L1 cells were treated for 10 days without insulin or with 10 μg/ml insulin with vehicle (*V*; Me_2SO, 1%), or the ligands at the indicated concentrations. After Oil Red O staining, the entire wells (*A*) or representative zones (*B*) were imaged. Triglyceride content was determined in cell lysates by colorimetric assay (500 nm) and normalized to the total quantity of protein measured by a Bradford assay (595 nm) (*C*). The same treatments were applied to wild type (*WT*) cells in the presence of the PPARγ antagonist GW9662 (*D*) and to 3T3L1 cells stably expressing an empty vector or a vector encoding an siRNA against PPARγ (*E*).

compared using a linear model allowing direct comparisons between the three conditions. The vast majority of the genes regulated by MEHP were also regulated by rosiglitazone (Fig. 7*A*), again indicating that the adipogenic actions of MEHP are mediated by PPARγ. Consistent with their ability to promote adipocyte differentiation, both compounds had strong effects on genes implicated in metabolism and cell cycle according to gene ontology analyses (Fig. 7*B*). The metabolic genes regulated by rosiglitazone and MEHP affected both catabolic and anabolic pathways (Table 1). Several genes implicated in glucose uptake, glycolysis, β-oxidation, citrate cycle, and oxidative phosphorylation were up-regulated, likely providing the cells with high energetic levels to fulfill anabolic functions. The treatments with MEHP and rosiglitazone also induced genes required for the structure of lipid droplets (*aP2* and *Adrp*) and the function of mature adipocytes (lipogenesis, triglyceride synthesis, and adipokines). Interestingly, we also observed an up-regulation of enzymes from the pentose phosphate pathway and from some intermediate steps of neoglucogenesis, which can potentially increase NADPH levels subsequently utilized for lipogenesis.

MEHP specifically regulated only a very low number of genes that could not be assigned to characterized adipocyte differentiation pathways. In contrast, rosiglitazone had a broader action than MEHP because around 30% of the genes were specifically regulated by this full agonist (Fig. 7*A*). Thus, MEHP potentially acts as a selective PPAR modulator regulating only a subset of PPARγ target genes compared with a full agonist. This target gene specificity could potentially translate into selective functional actions. However, genes specifically regulated by rosiglitazone were distributed within various pathways with no particular enrichment in a specific function (Fig. 7*B* and Table 1). This observation precludes concluding on the respective selective biological functions of rosiglitazone and MEHP. The physiological selectivity, if any, may therefore rather arise from a differential regulation of rate-limiting enzymes or of crucial proteins rather than an entire pathway.

To validate the concept of a selective modulation of PPARγ targets by MEHP, we analyzed the expression of well described PPARγ target genes by quantitative reverse transcriptase-PCR (Fig. 8 and Table 2). When differentiation was induced with rosiglitazone, most genes were up-regulated, from around 2-fold for PPARγ itself up to 400-fold for *OLR1* (Fig. 8*B*), whereas the expression of some described PPARγ targets

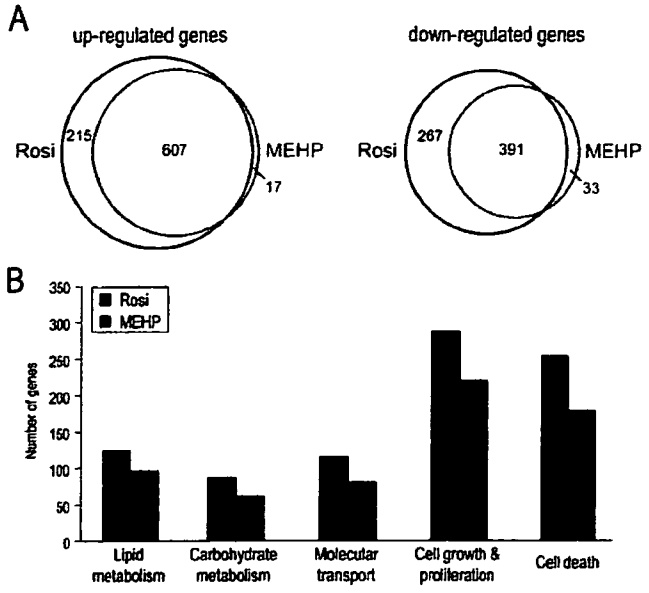

FIGURE 7. **MEHP regulates only a subset of genes compared with rosiglitazone.** RNA from 2-day post-confluent 3T3L1 cells treated for 10 days with 10 μg/ml insulin in combination with vehicle (*V*; Me_2SO, 1%), 1 μM rosiglitazone, or 100 μM MEHP was subjected to a custom microarray as described under "Experimental Procedures." Genes were considered to be significantly regulated when the *p* value was lower than 0.05 and the -fold change was above 2. The regulation by rosiglitazone and MEHP compared with the untreated control are summarized as Venn diagrams (*A*) and the significant gene ontology classes are represented for each condition (*B*).

remained unaffected (Table 2). When MEHP was used as a PPARγ ligand, 8 of 10 genes were similarly induced (*Pparγ*, *Fabp-4/aP2*, adiponectin (*Adipoq*), *Cd36*, acyl-CoA synthetase 1 (*Acs-1*), lipoprotein lipase (*Lpl*), *C/ebpα*, and liver X receptor α (*Lxrα*)), whereas *Gyk* and *Olr1* were significantly less induced, indicating that the efficacy of gene induction by MEHP depends on the promoter context. In addition, we confirmed new potential PPARγ targets from the microarray results by showing that expression of the lipogenic enzyme acetyl-CoA carboxylase β (*Accβ*) is induced both by MEHP and rosiglitazone, whereas that of acyl-CoA synthetase Bubblegum 1 (*Acsbg1*) is induced to higher levels with rosiglitazone than with MEHP.

In the experiment described above, PPAR ligands were added all along the differentiation process. Because the activity of PPARγ is intrinsically linked to adipocyte differentiation, it is therefore difficult to uncouple the direct induction of PPARγ target genes from their indirect activation via the global network of transcription factors controlling the adipogenic program. We hence performed the same gene expression analyses with 3T3L1 cells treated for 48 h with rosiglitazone or MEHP, either before differentiation or after differentiation with a classical adipogenic mixture, as described under "Experimental Procedures" (Fig. 8, *A* and *C*). Interestingly, the relative efficacy of MEHP compared with rosiglitazone varied between promoters and, for a given promoter, was different between the three differentiation status (non-differentiated, differentiated with a PPAR ligand, or differentiated with a classical mixture). When treatments were performed in differentiated adipocytes, target gene induction was globally reduced or alleviated (Fig. 8*C*), presumably because the expression of these genes was already high in differentiated cells. Nevertheless, genes such as *Gyk*, *Olr1*, *Acsbg1*, and *Fabp-4* that could still be further induced, maintained an activation profile whose selectivity was similar to that obtained with treatments during differentiation. In contrast, *Fabp-4* and *Adipoq*, which were strongly activated to equal levels both by MEHP and rosiglitazone in cells treated during differentiation, only responded to rosiglitazone in non-differentiated cells (Fig. 8*A*).

Altogether, these results demonstrate that in the same cellular context, MEHP exerts a selective action on different PPARγ target genes that varies according to the differentiation status of the cell. Two different classes of genes must be distinguished. The first group includes genes such as *Gyk*, *Olr1*, and *Acsbg1* on which MEHP exerts a lower activity than rosiglitazone, independently of the differentiation status of the cell. A second group is exemplified by *Fabp-4* and *Adipoq*, which equally respond to MEHP and rosiglitazone during differentiation but are principally induced by rosiglitazone in undifferentiated cells.

DISCUSSION

MEHP Induces Adipogenesis by Activating PPARγ—The activation of PPARγ by the phthalate monoester MEHP, a metabolite of the industrial pollutant DEHP, has been previously reported (20, 21). However, these experiments, conducted in a toxicological perspective, did not address the molecular mechanisms of action as well as the physiological consequences of such an activation. We demonstrated herein that MEHP-dependent PPARγ activation promotes adipocyte differentiation, whereas DEHP has no effect. Several lines of evidence suggest that the adipogenic properties of MEHP are mediated by PPARγ. First, MEHP concentrations required for minimal and maximal induction of adipogenesis parallel those required for PPARγ activation in transactivation assays. Second, the adipogenic actions of MEHP are reduced by knocking-down PPARγ or by inhibiting its activity with an antagonist, although the intricate link between PPARγ and adipogenesis does not totally rule out the possibility of a concomitant action of MEHP downstream of PPARγ. Third, when analyzed on a genome-wide basis, the majority of the genes regulated by MEHP during adipogenesis are also regulated by the full PPARγ agonist rosiglitazone. Finally, MEHP can induce the expression of some PPARγ target genes important for adipocyte differentiation. Nevertheless, this compound differs from thiazolidinediones by reduced affinity and efficacy and by eliciting a partial adipogenic response compared with rosiglitazone.

MEHP Selectively Regulates PPARγ Activity during Adipogenesis—Modelization of MEHP within the PPARγ LBD revealed a configuration very similar to rosiglitazone. However, the conformational changes induced by both ligands or their ability to stabilize helix 12 in an active configuration are most likely different because MEHP promotes interactions with only a subset of PPARγ coregulators. Indeed, using three independent tools, *i.e. in vitro*, in living cells and on PPARγ target promoters, we demonstrated that MEHP only partially induces corepressor release and promotes the recruitment of the coactivators Med1 and PGC-1α but not of p300 and SRC-1. In addi-

TABLE 1

The metabolic actions of MEHP and rosiglitazone during 3T3L1 differentiation

The table represents the -fold induction of significantly regulated metabolic genes from the microarray analysis described in Fig. 3. Genes that are regulated by rosiglitazone only are in red and genes regulated by both ligands with a statistically higher effect with rosiglitazone are in green.

Lipid metabolism	Rosi vs V	MEHP vs V
β-oxidation:	(fold change)	(fold change)
Acyl-CoA dehydrogenase, C-2 to C-3 short chain	3.5	2.8
Acyl-CoA dehydrogenase, medium chain fatty acid	2.9	2.4
Acyl-CoA dehydrogenase, long chain	3.0	3.1
Acyl-CoA dehydrogenase, very long chain	3.8	3.4
Carnitine palmitoyltransferase 1B	4.9	6.7
Carnitine palmitoyltransferase 2	2.9	3.4
Enoyl-CoA hydratase 1 (peroxisomal)	2.3	-
Enoyl Coenzyme A hydratase, short chain, 1, mitochondrial	2.2	2.3
Acyl-CoA oxidase 1	6.7	5.3
Acyl-CoA synthetase long-chain family member 1	10.0	9.2
Acyl-CoA synthetase long-chain family member 4	3.1	3.0
Acyl-CoA synthetase subfamily member 1	7.5	3.5
HADHA	3.9	3.4
Acetyl-CoA acetyltransferase 2	2.7	2.6
Lipogenesis		
Acetyl-Coenzyme A carboxylase beta	6.1	5.6
Fatty acid synthase	2.1	2.4
Triglyceride synthesis		
Glycerol-3-Phosphate-dehydrogenase	7.1	5.1
Glycerol Kinase	5.8	3.8
Phosphatidate phosphatase 2B	-2.2	-2.5
Diacylglycerol O-acyltransferase homolog 1	5.1	3.7
Diacylglycerol O-acyltransferase homolog 2	2.7	2.8
Ketone body metabolism		
Hydroxyacyl-CoA dehydrogenase	2.5	2.1
Adipokines and adipokine signaling:		
Adipsin	2.1	-
Adiponectin	6.5	5.5
Adiponectin receptor 2	8.2	6.2
Visfatin (PBEF1)	3.9	3.9
Angiopoietin-like 4 (FIAF)	3.8	4.0
MCP-1 (CCL 13)	-3.8	-3.7
Il-5	2.5	
Malonyl CoA/AMPK signaling:		
Malonyl-CoA decarboxylase	3.1	2.5
Others		
Lipoprotein lipase (LPL)	4.1	3.7
CD36	10.2	10.0
Hormone-sensitive lipase (HSL)	7.4	5.7
Lipase, member H	2.3	-
Apolipoprotein C-II	2.1	-
Apolipoprotein B editing complex 1 (Apobec1)	2.6	2.5
Fatty acid desaturase 1	2.4	2.5
Low density lipoprotein receptor	2.6	2.9
Low density lipoprotein-related protein 1	2.9	2.6
Methylmalonyl-Coenzyme A mutase	2.2	2.2
Fatty acid binding protein 4; adipocyte (aP2)	10.1	9.4
Adipose differentiation-related protein (ADRP)	6.6	5.5
Nuclear receptor signaling		
PPARa	2.2	-
RXRa	2.2	
NCOR2	-2.3	-
PGC-1a	2.1	2.1
PGC-1b	6.8	5.8
LXRa	4.9	3.8
ERRa	2.6	2.3
NR2F1(COUP TF1)	-3.3	-2.0
Citrate cycle		
aconitase 1, soluble	3.2	2.8
aconitase 2, mitochondrial	3.7	3.1
citrate synthase	5.1	4.6
fumarate hydratase	2.4	2.2
isocitrate dehydrogenase 3 (NAD+) alpha	6.8	6.2
isocitrate dehydrogenase 3 (NAD+) gamma	2.4	2.2
malate dehydrogenase 1, NAD (soluble)	4.2	3.7
malate dehydrogenase 2, NAD (mitochondrial)	2.6	2.3
oxoglutarate (alpha-ketoglutarate) dehydrogenase (lipoamide)	2.9	2.6
pyruvate carboxylase	4.3	4.6
succinate dehydrogenase complex, subunit A	2.6	2.5
succinate dehydrogenase complex, subunit B	2.2	2.2
succinate dehydrogenase complex, subunit D	2.7	2.3
succinate-CoA ligase, ADP-forming, beta subunit	2.8	2.7
succinate-CoA ligase, GDP-forming, alpha subunit	2.8	2.6

Specifically regulated by Rosiglitazone

HADHA = Hydroxyacyl-Coenzyme A dehydrogenase/3-ketoacyl-Coenzyme A thiolase/enoyl-Coenzyme A hydratase, alpha subunit

Carbohydrate metabolism	Rosi vs V	MEHP vs V
Glycolysis:	(fold change)	(fold change)
Hexokinase 2	7.2	6.8
Glucose phosphate isomerase 1	4.8	4.5
Phosphofructokinase	4.4	5.2
Fructose-bsphosphate Aldolase A	3.6	3.6
Fructose-bsphosphate Aldolase B	2.5	2.4
Fructose-bsphosphate Aldolase C	7.0	5.0
Triosephosphate isomerase 1	3.5	3.3
Phosphoglycerate mutase 2	3.0	2.9
Phosphopyruvate hydratase	2.2	2.0
Pyruvate kinase	2.2	2.1
Pyruvate dehydrogenase b	2.8	2.4
Pyruvate dehydrogenase kinase, isoenzyme 1	4.9	4.9
Pyruvate dehydrogenase kinase, isoenzyme 4	9.1	7.1
Phosphoglycerate kinase	4.3	4.2
Glyceraldehyde-3-P dehydrogenase	5.4	4.6
Neoglucogenesis:		
PEPCK 1	20.4	18.8
Fructose-1,6-bisphosphatase 1	2.0	-
Fructose-1,6-bisphosphatase 2	2.1	2.1
Pyruvate carboxylase	3.5	3.4
Malate dehydrogenase 1 (soluble)	4.3	3.6
Malate dehydrogenase 1 (mitochondrial)	2.4	2.2
Glycerol-3-phosphate dehydrogenase 1	7.1	5.1
Pentoses phosphate pathway		
Glucose-6-Phosphate dehydrogenase	2.1	2.1
Transketolase	2.6	2.4
Transketolase like 1	2.2	-
Transaldolase 1	3.4	2.9
Hexosamine biosynthetic pathway:		
Glutamine-fructose-6-phosphate transaminase 1	3.0	2.4
Glucosamine-P N-acetyltransferase 1	2.3	2.9
Glutamine synthase	3.0	
Insulin signaling:		
IRS-2	4.1	3.4
IRS-4	7.5	6.0
Protein tyrosine phosphatase (NS1)	2.1	-
PI3KR1 (phosphoinositide-3-kinase, regulatory subunit 1)	-2.1	-
PI3KR2	2.1	
AKT1	2.3	
Serum/Glucocorticoid regulated kinase	-2.7	-2.2
PKC iota	2.1	-
Glut4	12.5	12.8
Syntaxin binding protein 4	2.7	
PKAb	4.8	4.5
Lipase hormono-sensible	5.8	7.4
Oxidative phosphorylation		
Complex I:		
NADH dehydrogenase 1 alpha subcomplex 10	2.3	2.0
NADH dehydrogenase (ubiquinone) 1 beta subcomplex 9	2.6	2.4
NADH dehydrogenase (ubiquinone) 1 subcomplex 2	2.5	2.3
NADH dehydrogenase (ubiquinone) Fe-S protein 1	2.2	2.0
NADH dehydrogenase (ubiquinone) Fe-S protein 2	2.1	2.0
NADH dehydrogenase (ubiquinone) Fe-S protein 3	2.1	
NADH dehydrogenase (ubiquinone) Fe-S protein 7	2.5	2.2
NADH dehydrogenase (ubiquinone) flavoprotein 1	2.8	2.8
NADH dehydrogenase (ubiquinone) flavoprotein 2	2.4	2.0
NADH dehydrogenase (ubiquinone) 1 beta subcomplex 5	2.3	2.0
Complex II:		
Succinate dehydrogenase complex, subunit A	2.5	2.4
Succinate dehydrogenase complex, subunit B	2.1	2.1
Succinate dehydrogenase complex, subunit C	2.5	2.2
Complex III:		
Cytochrome c-1	4.1	3.3
Ubiquinol-cytochrome c reductase core protein I	2.7	2.5
Ubiquinol-cytochrome c reductase core protein II	3.3	2.3
Ubiquinol-cytochrome c reductase, Rieske iron-sulfur polypeptide 1	4.5	3.7
Ubiquinol-cytochrome c reductase hinge protein	2.5	2.1
Complex IV:		
Cytochrome c oxidase subunit IV isoform 1	2.4	2.3
Cytochrome c oxidase subunit VIa polypeptide 1	2.6	2.2
Cytochrome c oxidase subunit VIIa polypeptide 1 (muscle)	2.3	
Cytochrome c oxidase subunit VIIa polypeptide 2 (liver)	2.8	2.2
Cytochrome c oxidase subunit 6A (ubiquitous)	2.3	
ATP synthase:		
ATP5A1	2.1	-
ATP5B	2.9	2.7
ATP5C1	2.1	
ATP5D	2.7	2.3
ATP5F1	2.0	2.0
ATP5G1	2.2	-
Pyrophosphatase (inorganic) 1	8.7	6.1

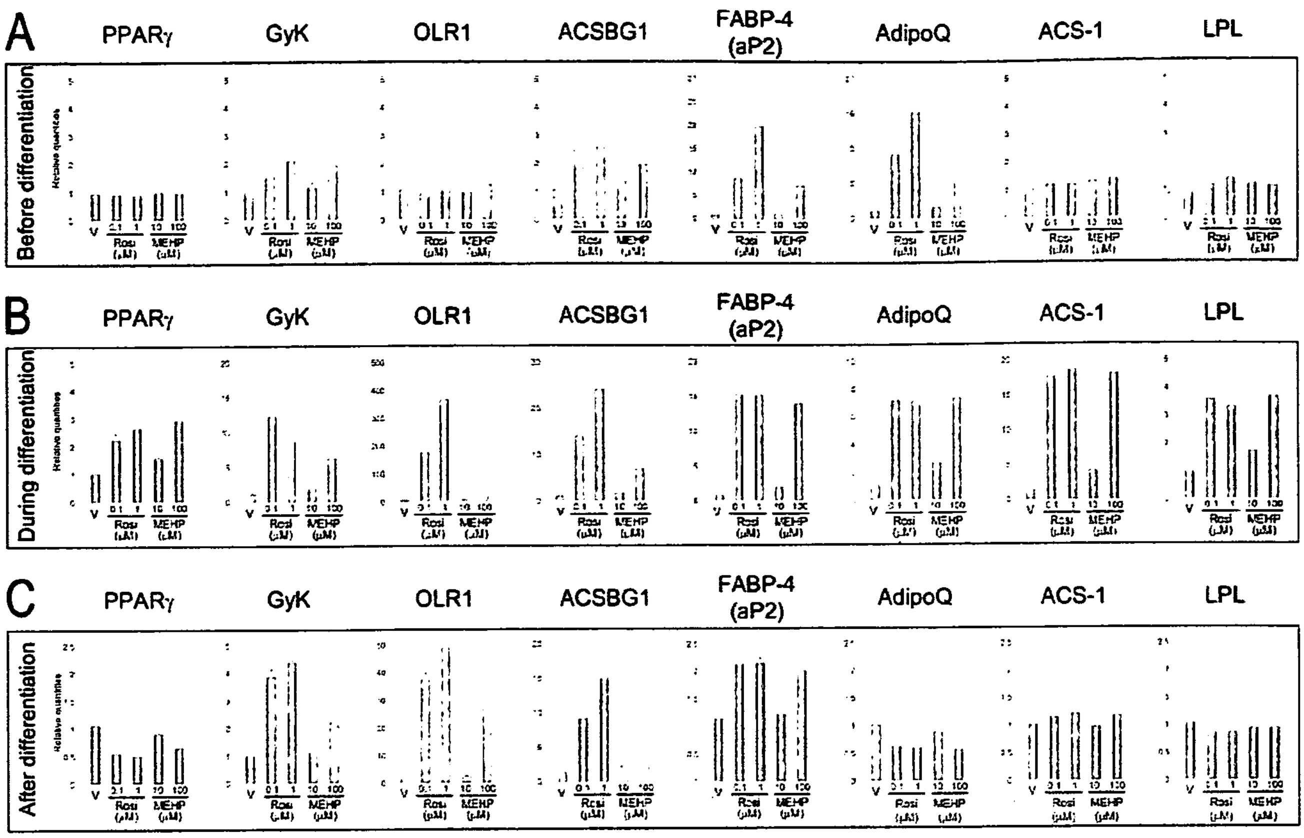

FIGURE 8. **MEHP selectively induces PPARγ target genes in a differentiation-dependent manner.** 3T3L1 cells were treated with a combination of 10 μg/ml insulin and vehicle (*V*; Me_2SO, 1%), rosiglitazone, or MEHP at the indicated concentrations. The treatments were performed for 48 h in growing non-differentiated cells (*A*), for 10 days in 2-day post-confluent cells (*B*), and for 48 h in cells initially differentiated during 10 days with an adipogenic mixture devoid of PPARγ ligand as described under "Experimental Procedures" (*C*). Gene expression levels relative to three housekeeping genes were quantified by TaqMan quantitative reverse transcriptase-PCR. Abbreviations are: *Gyk*, glycerol kinase; *OLR1*, oxidized low density lipoprotein receptor 1; *FABP*, fatty acid-binding protein; *Adipoq*, adiponectin; *ACS*, acyl-CoA synthetase; *LPL*, lipoprotein lipase. Genes selectively induced during and after differentiation are represented in *green*, genes selectively induced before differentiation but non-selectively induced after differentiation are represented in *blue*, and genes only induced during differentiation and in a non-selective manner are represented in *red*.

TABLE 2

MEHP selectively induces PPARγ target genes in a differentiation-dependent manner

The results from Fig. 4 are presented as -fold inductions over vehicle treatment and extended to additional genes.

	Before differentiation (fold induction over vehicle treatment)				During differentiation[1] (fold induction over vehicle treatment)				After differentiation[2] (fold induction over vehicle treatment)				
	Rosiglitazone		MEHP		Rosiglitazone		MEHP		Rosiglitazone		MEHP		
	100nM	1μM	10μM	100μM	100nM	1μM	10μM	100μM	100nM	1μM	10μM	100μM	
PPARγ	1.0	1.0	1.1	1.0	2.2	2.6	1.6	2.9	0.5	0.5	0.9	0.6	
GyK	1.4	1.5	1.6	1.7	13.3	[illegible]	[illegible]	[illegible]	[illegible]	4.6	1.1	[illegible]	Genes selectively induced during [illegible]
OLR1	[illegible]	[illegible]	[illegible]	1.2	225.6	[illegible]	[illegible]	[illegible]	[illegible]	[illegible]	[illegible]	[illegible]	
ACSBG1	7.4	12.2	[illegible]	4.7	15	27.5	[illegible]	[illegible]	[illegible]	[illegible]	[illegible]	[illegible]	
FABP-4/aP2	9.9	23.1	1.2	8.2	22.6	23.8	2.5	20.6	1.9	1.9	1.1	1.8	Genes selectively induced before differentiation but non-selectively induced after differentiation
AdipoQ	8.3	14.0	1.4	4.7	7.4	7.3	2.5	7.4	0.6	0.6	0.9	0.6	
CD36/FAT	48.3	119.0	2.4	40.1	17.7	20.5	2.7	21.0	1.0	1.1	0.8	1.1	
ACS-1	[illegible]	[illegible]	1.1	1.3	13.6	14.5	2.7	13.3	1.2	1.2	[illegible]	1.2	Genes only induced during differentiation and in a non-selective manner
LPL	1.1	1.3	1.1	1.0	3.8	3.7	2.0	4.4	[illegible]	0.8	0.9	0.9	
ACCβ	1.4	1.3	1.1	1.3	3.1	2.9	1.3	2.6	1.4	1.3	1.1	1.3	
C/EBPα	1.4	1.7	1.2	1.5	6.2	6.4	1.9	5.7	N.D.	N.D.	N.D.	N.D.	
LXRα	1.3	3.0	1.0	2.1	5.4	6.5	2.1	5.7	[illegible]	0.8	0.8	0.7	
SMRT	0.7	0.8	0.9	0.7	0.8	0.8	1.1	0.7	0.5	0.8	0.9	0.7	Others
FATP	1.3	0.9	1.0	1.1	0.9	1.0	1.2	1.1	N.D.	N.D.	N.D.	N.D.	

[1] Cells were differentiated with the indicated ligands in the presence of insulin.

[2] Cells were induced with a differentiation cocktail for 2 days (isobutylmethylxanthine/dexamethasone/insulin), differentiated for 8 days with insulin and then treated with the indicated ligands.

tion, other coregulators may be selectively recruited by MEHP and rosiglitazone. This is indeed reflected by the partial reduction of PPARγ mobility upon MEHP treatment in living cells where a full set of coactivators is present and where the reduction of PPAR mobility upon ligand binding is governed by the engagement in large complexes of coregulators (8, 9).

This selective recruitment of coregulators translates into a partial adipogenic program where only a subset of genes is regulated by MEHP compared with rosiglitazone. The partial release of NCoR in response to MEHP seems sufficient to alleviate the inhibitory effects of this corepressor on most PPARγ targets to promote adipogenesis (41). Indeed, genes important for adipocyte differentiation (*Fabp-4*, *adiponectin*, *Acs*, and *Lpl* among others) are fully induced. In contrast, other direct PPARγ targets such as *Gyk*, *Olr1*, and *Acsbg1* are only partially activated by MEHP. Interestingly, *Gyk* and *Olr1* are specifically silenced by corepressors during adipogenesis and require an exogenous PPARγ ligand for activation (10, 40) (Fig. 5). Thus, the low levels of PPARγ/NCoR interaction remaining upon MEHP binding could limit the maximal activation level of such genes. In contrast, genes such as *Fabp-4* whose promoter is never associated with corepressors are insensitive to the limited action of MEHP on corepressor release, thereby potentially explaining why such genes are equally activated by MEHP and rosiglitazone. *Adipoq* is also activated by MEHP and rosiglitazone with equal efficacy. Amazingly, the persistence of NCoR on the *Adipoq* promoter in the presence of MEHP, as well as in the presence of rosiglitazone albeit to a lower level, has to be compensated by stronger levels of coactivator recruitment such as those observed on this promoter for PGC-1α. The selective recruitment of coactivators may also play a role in the differential induction of target genes. Although we have not observed major promoter-specific differences in the association of the coactivators tested here, it is possible that subtle differences between promoters may explain differences in gene expression. In addition, the reduced adipogenic potential of MEHP compared with rosiglitazone could also be linked to a reduced efficacy in the recruitment of some coactivators. Indeed, both in live cell FRET assay and in chromatin immunoprecipitation experiments, MEHP induced only a partial recruitment of Med1, a coactivator required for efficient adipocyte differentiation (42).

Distinguishing Selective PPARγ Modulation from Partial PPARγ Activation—Using MEHP as a model, this study demonstrates the molecular basis of selective PPAR modulation and clearly establishes the difference between selective PPAR modulators and partial PPARγ agonists. SPPARMs are usually characterized by their molecular properties, *i.e.* the ability to induce selective coregulator recruitment (14). This is then related to a physiological output where a restricted PPARγ action is established. Between these two steps, the nature of the target gene regulation is, however, often underevaluated. Indeed, when compared with full agonists, SPPARMs differ from partial agonists as they promote selective gene regulation by differentially affecting target gene transcription in a gene-specific manner, with some genes induced to similar levels than those obtained with a full agonist, whereas others exhibit restricted activation. In contrast, partial agonists exhibit a global decrease in the activation of all target genes. Thus, a bona fide SPPARM should induce conformational changes different from full agonists that translate into selectivity in terms of coregulator interactions, target gene induction, and ultimately physiological effects. At the molecular level, MEHP fulfills these conditions as the differential recruitment of coregulators translates into a restricted profile of gene regulation.

Our results also point to the importance of the cellular context regarding coregulator equipment, illustrated by the differences of PPARγ transactivation by MEHP according to the cell line analyzed. In addition, gene expression analyses on 3T3L1 cells treated with PPARγ agonists before, during, or after differentiation, suggest that both the level and the selectivity of target gene induction rely on the expression of distinct sets of coregulators. Thus, PPARγ agonists may exert different effects on subpopulations of adipocytes and their progenitors in the adipose tissue, an aspect that should be taken into consideration in pharmacological strategies aimed at finding PPARγ modulators acting on adipocyte physiology.

The identification of SPPARMs that favor the beneficial pharmacological actions of thiazolidinediones over their adverse effects is a major challenge for pharmaceutical research on type 2 diabetes (13, 43), for which some candidate compounds are starting to emerge (44–48). FK614 is a SPPARM causing impaired recruitment of CREB-binding protein but retaining beneficial effects on insulin sensitivity in hyperglycemic mouse models (46, 49, 50). The inability of MEHP to promote interactions between PPARγ and p300, a coactivator highly homologous to CREB-binding protein, and enhanced recruitment of PGC-1α would both potentially be compatible with a positive action of MEHP on insulin sensitivity (45, 50). However, a metabolic study of phthalate exposure in animal models is required to understand how the molecular and cellular effects described herein potentially translate into the selective regulation of the physiological functions regulated by PPARγ. Whereas mice and rats are the models most often used for this type of metabolic studies, the occurrence of sustained hepatic peroxisome proliferation mediated by PPARα, which does not occur in humans, is likely to affect the final metabolic phenotype of these animals, and alternate models might have to be considered.

MEHP Is a Potential Metabolic Disruptor—Our results on the adipogenic action of MEHP strongly argue that in addition to an action on hepatic carcinogenesis through PPARα-mediated peroxisome proliferation (51), the endocrine disrupting actions of DEHP through its MEHP metabolite should also be considered with respect to the development of obesity and associated metabolic disorders. We have observed that human PPARγ can be activated with similar affinities and efficacies than the mouse isotype, but we failed to detect the subtle differences in affinity described by other reports that may therefore be linked to the cellular context (20, 21). In addition, MEHP induces the same pattern of coregulator recruitment with the mouse and human receptors, suggesting that the effects of MEHP on adipogenesis studied here in the context of the mouse receptor may translate into similar effects in humans if MEHP reaches the adipose tissue in sufficient concentration. Although the human exposure to DEHP is ubiquitous through daily products, plasmatic levels of both DEHP and MEHP generally remain low because of rapid urinary excretion (17). However, individuals requiring frequent blood transfusion or dialysis are subjected to repetitive acute exposures to high levels of DEHP because of the leaching of the compound from plastic

bags and tubings in direct contact with biological fluids. Under such circumstances, the plasmatic levels of DEHP and MEHP can reach 50 μM in humans (17), a concentration at which we already observed strong although not maximal induction of adipogenesis. Although the concentration of MEHP in adipocytes is difficult to assess, DEHP is lipophilic and can accumulate in adipose tissue (52, 53). Despite the absence of data available to our knowledge on MEHP accumulation in the adipose tissue or on the adipose tissue expression of lipases that metabolize DEHP into MEHP, our data combined with these observations urge the need to consider the actions of DEHP and MEHP in the pathophysiology of this tissue. Together with reports showing that other pollutants including different phthalate esters and organotins can also target PPARγ and promote adipogenesis in cellular models (20, 21, 54, 55) and *in vivo* (56), our study suggests that the metabolic functions of PPARγ can be targeted by a subclass of endocrine disruptors that we propose to define as metabolic disruptors.

Acknowledgments—We are grateful to Beatriz Tavera-Tolmo and Sandra Luecke for experimental work. We thank Braj and Vidya Lohray from the Zydus Research Centre for the synthesis of the GW9662 antagonist, members of the Lausanne DNA array facility for valuable technical help with microarray and qPCR experiments, and the VITAL-IT project of the Swiss Institute of Bioinformatics for providing computational resources.

REFERENCES

1. Waring, R. H., and Harris, R. M. (2005) *Mol. Cell Endocrinol.* **244,** 2–9
2. Markey, C. M., Rubin, B. S., Soto, A. M., and Sonnenschein, C. (2002) *J. Steroid Biochem. Mol. Biol.* **83,** 235–244
3. Henley, D. V., and Korach, K. S. (2006) *Endocrinology* **147,** Suppl. 6, S25–S32
4. Tabb, M. M., and Blumberg, B. (2006) *Mol. Endocrinol.* **20,** 475–482
5. Evans, R. M., Barish, G. D., and Wang, Y. X. (2004) *Nat. Med.* **10,** 355–361
6. Desvergne, B., Michalik, L., and Wahli, W. (2004) *Mol. Endocrinol.* **18,** 1321–1332
7. Lehrke, M., and Lazar, M. A. (2005) *Cell* **123,** 993–999
8. Feige, J. N., Gelman, L., Tudor, C., Engelborghs, Y., Wahli, W., and Desvergne, B. (2005) *J. Biol. Chem.* **280,** 17880–17890
9. Tudor, C., Feige, J. N., Pingali, H., Lohray, V. B., Wahli, W., Desvergne, B., Engelborghs, Y., and Gelman, L. (2007) *J. Biol. Chem.* **282,** 4417–4426
10. Guan, H. P., Ishizuka, T., Chui, P. C., Lehrke, M., and Lazar, M. A. (2005) *Genes Dev.* **19,** 453–461
11. Michalik, L., Zoete, V., Krey, G., Grosdidier, A., Gelman, L., Chodanowski, P., Feige, J. N., Desvergne, B., Wahli, W., and Michielin, O. (2007) *J. Biol. Chem.* **282,** 9666–9677
12. Feige, J. N., Gelman, L., Michalik, L., Desvergne, B., and Wahli, W. (2006) *Prog. Lipid Res.* **45,** 120–159
13. Berger, J. P., Akiyama, T. E., and Meinke, P. T. (2005) *Trends Pharmacol Sci.* **26,** 244–251
14. Gelman, L., Feige, J. N., and Desvergne, B. (2007) *Biochim. Biophys. Acta,* in press
15. Issemann, I., and Green, S. (1990) *Nature* **347,** 645–650
16. Lai, D. Y. (2004) *J. Environ Sci. Health C Environ. Carcinog. Ecotoxicol. Rev.* **22,** 37–55
17. NTP-CERHR Expert Panel (2000) *Di(2-ethylHexyl)Phthalate Report,* National Toxicology Program, United States Department of Health and Human Services, cerhr.niehs.nih.gov/chemicals/dehp/DEHP-final.pdf
18. Huber, W. W., Grasl-Kraupp, B., and Schulte-Hermann, R. (1996) *Crit. Rev. Toxicol.* **26,** 365–481
19. Lapinskas, P. J., Brown, S., Leesnitzer, L. M., Blanchard, S., Swanson, C., Cattley, R. C., and Corton, J. C. (2005) *Toxicology* **207,** 149–163
20. Bility, M. T., Thompson, J. T., McKee, R. H., David, R. M., Butala, J. H., Vanden Heuvel, J. P., and Peters, J. M. (2004) *Toxicol. Sci.* **82,** 170–182
21. Hurst, C. H., and Waxman, D. J. (2003) *Toxicol. Sci.* **74,** 297–308
22. Gelman, L., Zhou, G., Fajas, L., Raspe, E., Fruchart, J. C., and Auwerx, J. (1999) *J. Biol. Chem.* **274,** 7681–7688
23. Jeannin, E., Robyr, D., and Desvergne, B. (1998) *J. Biol. Chem.* **273,** 24239–24248
24. Nadra, K., Anghel, S. I., Joye, E., Tan, N. S., Basu-Modak, S., Trono, D., Wahli, W., and Desvergne, B. (2006) *Mol. Cell. Biol.* **26,** 3266–3281
25. Hellemans, J., Mortier, G., De Paepe, A., Speleman, F., and Vandesompele, J. (2007) *Genome Biol.* **8,** R19
26. Yang, Y. H., Dudoit, S., Luu, P., Lin, D. M., Peng, V., Ngai, J., and Speed, T. P. (2002) *Nucleic Acids Res.* **30,** e15
27. Smyth, G. K. (2004) *Stat. Appl. Genet. Mol. Biol.* **3,** Article3
28. Smyth, G. K., and Speed, T. (2003) *Methods* **31,** 265–273
29. Benjamini, Y., and Hochberg, Y. (1995) *J. R. Stat. Soc.* **57,** 289–300
30. Metivier, R., Penot, G., Hubner, M. R., Reid, G., Brand, H., Kos, M., and Gannon, F. (2003) *Cell* **115,** 751–763
31. Feige, J. N., Sage, D., Wahli, W., Desvergne, B., and Gelman, L. (2005) *Microsc. Res. Tech.* **68,** 51–58
32. MacKerell, A. D. (1998) *J. Phys. Chem.* **102,** 3586–3616
33. Halgren, T. (1995) *J. Comput. Chem.* **17,** 490–519
34. Cronet, P., Petersen, J. F., Folmer, R., Blomberg, N., Sjoblom, K., Karlsson, U., Lindstedt, E. L., and Bamberg, K. (2001) *Structure* **9,** 699–706
35. Berman, H. M., Battistuz, T., Bhat, T. N., Bluhm, W. F., Bourne, P. E., Burkhardt, K., Feng, Z., Gilliland, G. L., Iype, L., Jain, S., Fagan, P., Marvin, J., Padilla, D., Ravichandran, V., Schneider, B., Thanki, N., Weissig, H., Westbrook, J. D., and Zardecki, C. (2002) *Acta Crystallogr. Sect. D Biol. Crystallogr.* **58,** 899–907
36. Shi, G. Q., Dropinski, J. F., McKeever, B. M., Xu, S., Becker, J. W., Berger, J. P., MacNaul, K. L., Elbrecht, A., Zhou, G., Doebber, T. W., Wang, P., Chao, Y. S., Forrest, M., Heck, J. V., Moller, D. E., and Jones, A. B. (2005) *J. Med. Chem.* **48,** 4457–4468
37. Lee, M. S., Feig, M., Salsbury, F. R., Jr., and Brooks, C. L., 3rd (2003) *J. Comput. Chem.* **24,** 1348–1356
38. Nolte, R. T., Wisely, G. B., Westin, S., Cobb, J. E., Lambert, M. H., Kurokawa, R., Rosenfeld, M. G., Willson, T. M., Glass, C. K., and Milburn, M. V. (1998) *Nature* **395,** 137–143
39. Maloney, E. K., and Waxman, D. J. (1999) *Toxicol. Appl. Pharmacol.* **161,** 209–218
40. Chui, P. C., Guan, H. P., Lehrke, M., and Lazar, M. A. (2005) *J. Clin. Investig.* **115,** 2244–2256
41. Yu, C., Markan, K., Temple, K. A., Deplewski, D., Brady, M. J., and Cohen, R. N. (2005) *J. Biol. Chem.* **280,** 13600–13605
42. Ge, K., Guermah, M., Yuan, C. X., Ito, M., Wallberg, A. E., Spiegelman, B. M., and Roeder, R. G. (2002) *Nature* **417,** 563–567
43. Balint, B. L., and Nagy, L. (2006) *Endocr. Metab. Immune Disord. Drug Targets* **6,** 33–43
44. Berger, J. P., Petro, A. E., Macnaul, K. L., Kelly, L. J., Zhang, B. B., Richards, K., Elbrecht, A., Johnson, B. A., Zhou, G., Doebber, T. W., Biswas, C., Parikh, M., Sharma, N., Tanen, M. R., Thompson, G. M., Ventre, J., Adams, A. D., Mosley, R., Surwit, R. S., and Moller, D. E. (2003) *Mol. Endocrinol.* **17,** 662–676
45. Burgermeister, E., Schnoebelen, A., Flament, A., Benz, J., Stihle, M., Gsell, B., Rufer, A., Ruf, A., Kuhn, B., Marki, H. P., Mizrahi, J., Sebokova, E., Niesor, E., and Meyer, M. (2006) *Mol. Endocrinol.* **20,** 809–830
46. Minoura, H., Takeshita, S., Ita, M., Hirosumi, J., Mabuchi, M., Kawamura, I., Nakajima, S., Nakayama, O., Kayakiri, H., Oku, T., Ohkubo-Suzuki, A., Fukagawa, M., Kojo, H., Hanioka, K., Yamasaki, N., Imoto, T., Kobayashi, Y., and Mutoh, S. (2004) *Eur. J. Pharmacol.* **494,** 273–281
47. Rocchi, S., Picard, F., Vamecq, J., Gelman, L., Potier, N., Zeyer, D., Dubuquoy, L., Bac, P., Champy, M. F., Plunket, K. D., Leesnitzer, L. M., Blanchard, S. G., Desreumaux, P., Moras, D., Renaud, J. P., and Auwerx, J. (2001) *Mol. Cell* **8,** 737–747
48. Schupp, M., Clemenz, M., Gineste, R., Witt, H., Janke, J., Helleboid, S., Hennuyer, N., Ruiz, P., Unger, T., Staels, B., and Kintscher, U. (2005) *Diabetes* **54,** 3442–3452
49. Fujimura, T., Kimura, C., Oe, T., Takata, Y., Sakuma, H., Aramori, I., and

Mutoh, S. (2006) *J. Pharmacol. Exp. Ther.* **318,** 863–871
50. Fujimura, T., Sakuma, H., Konishi, S., Oe, T., Hosogai, N., Kimura, C., Aramori, I., and Mutoh, S. (2005) *J. Pharmacol. Sci.* **99,** 342–352
51. Rusyn, I., Peters, J. M., and Cunningham, M. L. (2006) *Crit. Rev. Toxicol.* **36,** 459–479
52. Williams, D. T., and Blanchfield, B. J. (1974) *Bull. Environ. Contam. Toxicol.* **11,** 371–378
53. Stein, M. S., Caasi, P. I., and Nair, P. P. (1973) *Environ. Health Perspect.* **3,** 149–152
54. Kanayama, T., Kobayashi, N., Mamiya, S., Nakanishi, T., and Nishikawa, J. (2005) *Mol. Pharmacol.* **67,** 766–774
55. Takeuchi, S., Matsuda, T., Kobayashi, S., Takahashi, T., and Kojima, H. (2006) *Toxicol. Appl. Pharmacol.* **217,** 235–244
56. Grun, F., Watanabe, H., Zamanian, Z., Maeda, L., Arima, K., Chubacha, R., Gardiner, D. M., Kanno, J., Iguchi, T., and Blumberg, B. (2006) *Mol. Endocrinol.* **20,** 2141–2155

Available online at www.sciencedirect.com
ScienceDirect
Toxicology in Vitro 21 (2007) 1066–1076
Toxicology in Vitro
www.elsevier.com/locate/toxinvit

Cytotoxicity of peroxisome proliferator-activated receptor α and γ agonists in renal proximal tubular cell lines

Héctor Giral, Ricardo Villa-Bellosta, Julia Catalán, Víctor Sorribas *

Laboratory of Molecular Toxicology, University of Zaragoza, E50013 Zaragoza, Spain

Received 7 August 2006; accepted 28 March 2007
Available online 14 April 2007

Abstract

Fibrates and thiazolidinediones are agonists of peroxisome proliferator-activated receptors (PPAR) α and γ, pharmacologically designed to control dyslipidemia and insulin resistance, respectively. Several works have reported the toxicity of some agonists in a number of tissues. In this work we have analyzed the toxicity of two PPARα (WY14643 and clofibrate) and two PPARγ (pioglitazone and ciglitazone) agonists, using three different renal proximal tubular cell lines: Opossum OK, pig LLC-PK1, and murine MCT. Cell death was determined by the activity of intracellular lactate dehydrogenase. WY14643 and ciglitazone increased cell death with LC_{50} values of 92–124 μM and 8.6–14.8 μM, respectively, depending on the cell line. Clofibrate and pioglitazone were, however, non-cytotoxic even at concentrations of 10 and 100 higher than the corresponding EC_{50}, which suggests that cell death is independent of PPAR activation. Discrimination between apoptosis or necrosis was analyzed by light microscopy and stress fiber morphology, double staining with acridine orange and ethidium bromide, binding of annexin V, caspase-3 activity, and DNA laddering. With these methods, no signs of apoptosis were observed, which suggests a direct necrosis of the compounds on these renal proximal tubular cell lines.

Keywords: PPAR; Peroxisome proliferator; WY14643; Clofibrate; Ciglitazone; Pioglitazone; Proximal tubule; Cytotoxicity; OK cells; LLC-PK1; MCT; Kidney

1. Introduction

Dyslipidemias and type II diabetes are two major alterations with dramatic effects in kidney function. Peroxisome proliferator-activated receptors (PPAR) are nuclear receptors that have been pharmacologically targeted to treat such metabolic disorders (Berger and Moller, 2002). Once activated by the corresponding ligands, PPARs heterodimerize with the retinoid X receptor and induce the expression of target genes. Fibrates are amphipathic carboxylic acids that have been used as agonists of PPARα to normalize hypertriglyceridemia (Robillard et al., 2005; Barter and Rye, 2006), while thiazolidinediones (TZDs) activate PPARγ to reduce the resistance of peripheral tissues to insulin (Staels and Fruchart, 2005; Musi and Goodyear, 2006). In addition to the activation of the corresponding PPARs, fibrates and TZDs also exert important effects in a PPAR-independent way. For example, troglitazone induces changes in the control of the activity of acid–base balance in LLC-PK1 through the activation of protein kinase C-ERK pathways (Welbourne et al., 2003).

Abbreviations: CHAPS, [(3-cholamidopropyl)dimethylammonio]-1-propanesulfonate hydrate; DIC, differential interference contrast; DMEM, Dulbecco's Modified Eagle Media; DMSO, dimethyl sulfoxide; DTT, dithiothreitol; EDTA, ethylenediaminetetraacetic acid; EGFP, enhanced green fluorescent protein; FCS, fetal calf serum; HBSS, Hank's balanced salt solution; Hepes, 4-(2-Hydroxyethyl)piperazine-1-ethanesulfonic; LC, lethal concentration; LDH, lactate dehydrogenase; PBS, phosphate-buffered saline; PI, propidium iodide; PPAR, peroxisome proliferator-activated receptor; RT-PCR, Reverse transcription-polymerase chain reaction; TBE, tris-borate-EDTA; TRITC, tetramethylrhodamine isothiocyanate; TZD, thiazolidinedione.

* Corresponding author. Tel.: +34 976761631; fax: +34 976761612.
E-mail address: sorribas@unizar.es (V. Sorribas).

0887-2333/$ - see front matter © 2007 Elsevier Ltd. All rights reserved.
doi:10.1016/j.tiv.2007.03.021

All PPARs identified so far have also been described in the kidney, either along the nephron or in non-parenchymal cells (Guan and Breyer, 2001; Sato et al., 2004). Several protective effects of both fibrates and TZDs have also been reported in the kidney, in addition to the effects on dyslipidemias and antidiabetic goals. Some of these effects involve correction of blood pressure in diabetic patients with hypertension, reduction in the progression of glomerulosclerosis, and correction of the ischemia-reperfusion injury (Izzedine et al., 2005; Chung et al., 2005). However, the kidney could be also a target for undesirable side effects of fibrates and TZD.

In recent years there have been numerous reports on the toxicity of PPAR agonists in several tissues, and this has been reviewed recently (Peraza et al., 2006). The toxic effects of PPARs include hepatocarcinogenicity, partially related to their activation by environmental pollutants. The agonists act as promoters depending on critical factors that include species differences in receptor activity, relative ligand binding/activation, and receptor specificity (reviewed by Klaunig et al., 2003). With respect to non-carcinogenic effects, they include cell proliferation reduction and an increase in apoptotic cell death in a variety of cell types (Arici et al., 2003; Liu et al., 2004; Tsuchiya et al., 2003; Roberts et al., 2002). Curiously, the renal toxicity of these drugs has not been extensively analyzed, and there are only a few reports available. For example, Weissgarten et al. (2006) reported decreased proliferation and increased apoptosis in mesangial cells obtained from mice treated with rosiglitazone, a PPARγ agonist. Similar findings have been obtained with renal fibroblasts (Parameswaran et al., 2003; Zafiriou et al., 2005), proximal tubular cells (Arici et al., 2003), and rat mesangial cells (Tsuchiya et al., 2003).

In this work, we have analyzed the cytotoxicity of two fibrates (WY14643 and clofibrate) and two thiazolidinediones (pioglitazone and ciglitazone) in several renal cell lines of proximal tubular origin. Clofibrate and pioglitazone showed no signal of toxicity even at supra-pharmacological doses, while WY14643 and ciglitazone induced a dose-dependent, non-apoptotic cell death at doses close to the dissociation constant of the compounds.

2. Materials and methods

2.1. Cell culture

Opossum kidney (OK) and pig LLC-PK1 (an appreciated donation from Dr. S.A. Kempson, Indiana University School of Medicine, Indianapolis) cells were grown identically, as previously described (Sorribas et al., 1995; Andreoli et al., 1993). In brief, they were cultured in a humidified 5% CO_2/95% air atmosphere in DMEM: Ham's F-12 (1:1, vol:vol) supplemented with 10% fetal calf serum (FCS), 100 IU/ml penicillin G and 100 μg/ml streptomycin, and 4 mM L-glutamine. Mouse cortical tubular cells (MCT, generously provided by Dr. M. Levi, University of Colorado HSC, Denver) were grown in DMEM supplemented with 10% FCS, 100 IU/ml of penicillin G, 100 μg/ml of streptomycin and L-glutamine. All three cell lines were grown to confluence and then rendered quiescent overnight by incubating the cells in the same corresponding culture media with 0.2% FCS.

2.2. Incubations with PPAR agonists

Quiescent cells were treated with PPAR ligands in Hank's balanced salt solution (HBSS) containing calcium and magnesium (Invitrogen, Carlsbad, CA) for the indicated times and concentrations of drugs. Similar results were obtained when the cells were incubated in DMEM. Two fibrates, WY14643 (Sigma, St. Louis, MO) and clofibrate (Calbiochem, San Diego, CA), were used as PPARα activators, and two TZDs, ciglitazone (Calbiochem) and pioglitazone (Cayman, Ann Arbor, MI), were used as PPARγ activators. All of them were dissolved in dimethyl sulfoxide (DMSO) prior to use, and a similar volume of DMSO was added to the control cells.

2.3. Lactate dehydrogenase (LDH)

Total cell death was quantified by the activity of the lactate dehydrogenase released from the cytosol of damaged cells into the supernatant of the cultures. In short, tubular epithelial cell lines were grown in 24-well plates and, when confluent, treated with the corresponding drugs in 1 ml assay medium. At the indicated times, 50 μl of medium were taken to measure LDH activity, and samples were kept at −20 °C until the assay. The activity was determined using a Cytotoxicity Detection kit (Roche, Mannheim, Germany) in a DTX-880 multimode plate reader (Beckman Coulter, Inc., Fullerton, CA), following the manufacturer's instructions. The assay is based on the reduction of NAD^+ to $NADH/H^+$ by the LDH-catalyzed conversion of lactate to pyruvate. Next, the enzyme diaphorase transfers H/H^+ from $NADH/H^+$ to iodotetrazolium chloride, which is reduced to formazan, which shows a broad absorption maximum at about 500 nm. The results are expressed as a percentage of total activity released with 2% Triton X-100 in assay medium. In dose–response experiments, the following equation expressing a sigmoidal curve with variable slope was used to calculate the mean lethal concentration (LC_{50}) by non-linear regression: $Y = LC_0 + (LC_{max} - LC_0)/(1 + 10^{((\log LC_{50} - X)*n)})$. In this equation, Y is the percentage of LDH activity, LC_0 is the percentage of activity at zero concentration of drug, LC_{max} is the maximal LDH activity as obtained with 2% Triton X-100, X is the logarithm of drug concentration, and n is the Hill slope. Activity was normalized according to the 100% activity obtained with triton X-100. Y starts at LC_0 and goes to LC_{max} with a sigmoid shape. GraphPad Prism 4.0 software for Macintosh was used for iterations and for kinetic and statistical analysis.

2.4. Phalloidin staining

Stress fibers were stained with TRITC (tetramethylrhodamine isothiocyanate)-conjugated phalloidin (Sigma), previously dissolved in methanol. Cells were grown on cover glasses, and after treatment of the cells with the corresponding PPAR activators they were washed with phosphate-buffered saline (PBS), fixed with 3% paraformaldehyde in PBS, and permeabilized with 0.1% saponin in PBS as previously described (Lanaspa et al., 2007). TRITC-phalloidin was added at 10 μg/ml for 30 min at room temperature to stain the actin filaments, and the cells were visualized using a Carl Zeiss Axiovert 200M (Jena, Germany) inverted fluorescence microscope.

2.5. Assay of cell viability with ethidium bromide-acridine orange uptake

Total cell death and distinction between early or late apoptosis and necrosis were determined by the differential uptake of these fluorescent DNA binding dyes exactly as previously described, but using adherent LLC-PK1 cells (McGahon et al., 1995). In brief, cells grown on cover glasses were incubated with 100 μl of a mixture of 4 μg/ml acridine orange (Fluka, Buchs, Switzerland) and 4 μg/ml ethidium bromide (Bio-Rad, Hercules CA) in PBS, after the corresponding treatments. Immediately the cells were visualized by fluorescent microscopy with a 488-nm excitation dichroic filter. Since acridine orange intercalates in the DNA but only interacts with the RNA, and viable cells do not uptake ethidium bromide, these cells exhibit green nuclei and a dotted-orange cytoplasm. However, ethidium bromide is taken up by necrotic cells, which turn red. With respect to early apoptotic cells, their nuclei remain green because ethidium bromide still cannot enter into them, whereas late apoptotic cells turn red due to the condensed chromatin. As a positive control for apoptosis in LLC-PK1 cells, cadmium was used at 50 μM for 16 h (data not shown).

2.6. Annexin V-propidium iodide staining

Changes in the position of phosphatidylserine (an early event in apoptosis) were determined with an ApoAlert Annexin V kit (Clontech Laboratories, Inc., Mountain View, CA) following the manufacturer's protocol. A combination of enhanced green fluorescent protein (EGFP), of annexin V fusion protein (a 35.8-kDa protein that has a strong affinity for phosphatidylserine) and propidium iodide (PI) was used to differentiate between apoptosis and necrosis. With this method, apoptotic cells would show green staining in the plasma membrane, but dead cells would stain red since PI is also used, which crosses plasma membranes that have lost their integrity, as in the case of ethidium bromide. In short, 5×10^5 LLC-PK1 cells growing on cover glasses were treated with different PPAR ligands and then incubated with 0.2 μg annexin V and 0.5 μg propidium iodide in 200 μl binding buffer. After incubation of the cells for 15 min at room temperature in the dark, they were washed and fixed with 2% paraformaldehyde. Analysis was performed using an Axiovert 200M fluorescence microscope with a dual filter for fluorescein and rhodamine.

2.7. Caspase-3 activity

Cysteine-requiring aspartate protease-3 (caspase-3) activation is one of the earlier events in apoptosis. The activity was determined in LLC-PK1 cells after 3 h of treatments, with a colorimetric Caspase-3 Assay kit (Sigma), following the instructions provided. In short, 10^7 cells growing in 3.5-cm diameter Petri plastic dishes were lysed in 100 μl of a buffer containing 50 mM 4-(2-hydroxyethyl)piperazine-1-ethanesulfonic (Hepes) pH 7.4, 5 mM -[(3-cholamidopropyl)dimethylammonio]-1-propanesulfonate hydrate (CHAPS) and 5 mM dithiothreitol (DTT). Cell lysates were spun at 20,000*g* for 15 min at 4 °C, and 5 μl of supernatants were combined with 85 μl of assay buffer (20 mM Hepes pH 7.4, 0.1% CHAPS, 5 mM DTT, 2 mM ethylenediaminetetraacetic acid EDTA), and 10 μl of Caspase-3 substrate, acetyl-Asp-Glu-Val-Asp p-nitroanilide, and incubated overnight at 37 °C. Release of p-nitroanilide from the substrate was determined by absorbance at 405 nm using a DTX-880 plate reader (Beckman Coulter). Data are shown as absolute absorbances, and direct comparison to the control cells are shown. As a positive control, LLC-PK1 cells were treated with 50 μM $CdCl_2$ for 16 hours. This treatment increased caspase-3 activity 8.8 times compared to untreated cells.

2.8. DNA fragmentation

One of the late events in apoptosis is endonuclease cleavage of genomic DNA into internucleosomal fragments of approximately 200 bp integer multiples. This clearly differentiates from necrotic cell death, where unorganized DNA degradation takes place (Wyllie, 1980). Genomic DNA was obtained as described (Zhivotosky and Orrenius, 2003): 0.5×10^6 LLC-PK1 cells grown in plastic support were harvested and lysed with 20 μl of a buffer containing 2 mM EDTA, 100 mM Tris–HCl pH 8.0, and 0.8% (w/v) sodium lauryl sarcosine. RNA and proteins were enzymatically degraded, and the resultant DNA electrophoresed in 1.8% agarose tris-borate-EDTA (TBE) gel at 60 mA for 4 h. The gels were photographed under UV light using a Gel-Doc system (Bio-Rad).

2.9. RT-PCR

Total RNA from the LLC-PK1 cells was isolated using a Micro-to-Midi Total RNA Purification System

(Invitrogen), and the contaminating genomic DNA was eliminated using an Amplification Grade DNase I (Invitrogen). Reverse transcription (RT) was performed with a Superscript III First-Strand Synthesis system, followed by polymerase chain reaction (PCR). 459 and 496 base pair fragments from pig PPAR alpha and gamma, respectively, were amplified using a Thermus DNA polymerase (Biotools B&M Labs, Madrid, Spain) and the following primers (Invitrogen): For PPARα, sense AGG TCC GCA TCT TCC A, antisense AGA AAG ACG TCG TCG GG; and for PPARγ sense TCC GGA GGA CTA TCA GA, antisense GGC ATA CTC TGT GAT CTC C were used. Amplicons were visualized in an ethidium bromide-stained DNA agarose gel under UV and acquired using a Gel-Doc system (Bio-Rad).

2.10. Statistical analysis

The data are shown as means ± the standard error. The statistical significance was determined by either a Student's *t*-test or a one-way analysis-of-variance (ANOVA) and the Tukey multiple-comparison test, whereby $P < 0.05$ was considered significant. Experiments were performed 3–6 times with similar results. The number of experiments performed depended on whether the parameters to be determined were of qualitative or quantitative type.

3. Results

3.1. Dose–response relationships of PPARα and PPARγ agonists and cell viability

Dose–response experiments were performed in three different renal proximal tubular cell lines to compare PPAR ligand concentration and the leakage of cytosolic lactate dehydrogenase (LDH) as a measure of total cell death. Dose–response assays were performed at different incubation times, and the results at the 12-hour time point are shown in Fig. 1.

With respect to PPARα agonists, clofibrate was inert up to 500 μM and for 12 h in all three cell lines (triangles, first row of panels). However, WY14643 induced a very sharp increase in LDH activity, especially in MCT cells (Hill coefficient 9.9), with a mean lethal concentration of approximately 100 μM in all three cell lines (squares, first row of panels). OK cells exhibited a smoother response but also the lowest observed experimental effect, with a significant increase in LDH activity at 50 μM WY14643. Similar findings were obtained with PPARγ agonists. A lower range of TZD concentrations was used, according to the dissociation constants of the drugs and the plasma therapeutic concentrations (Brunton et al., 2005). Pioglitazone did not increase LDH activity up to 50 μM (not shown), but ciglitazone induced cell death with an LC_{50} of approximately 10 μM. Again, MCT cells exhibited the steepest

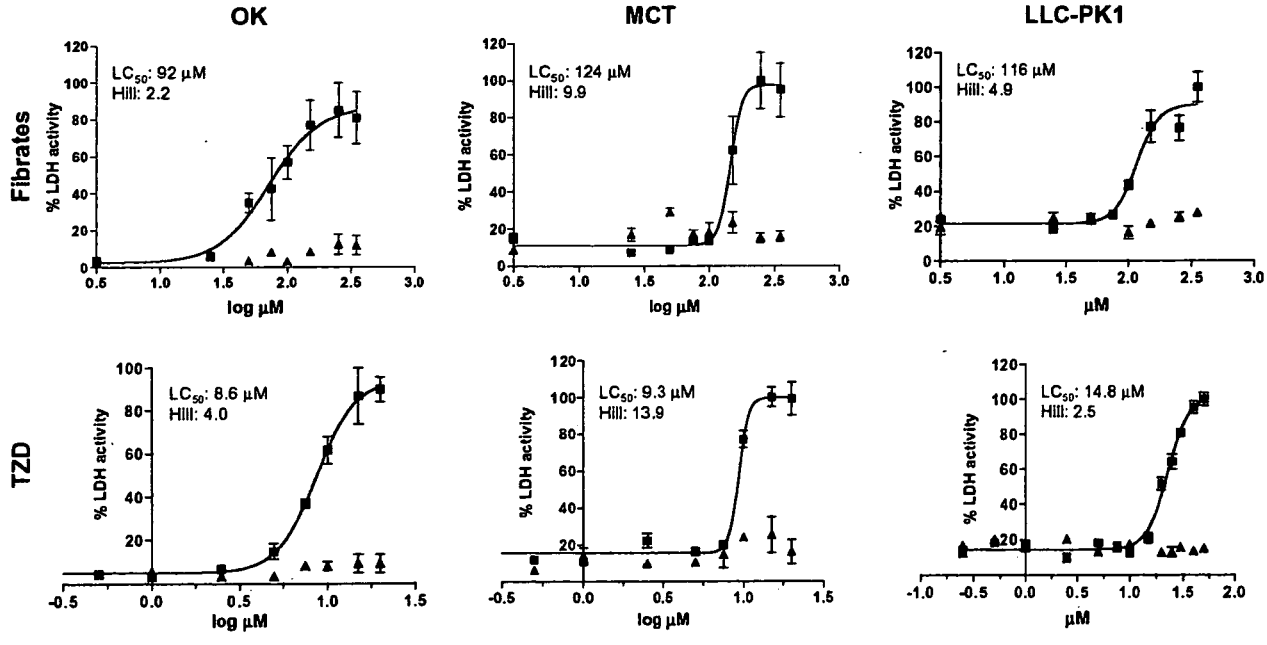

Fig. 1. Dose–response assays of LDH activity as a function of PPAR agonists, fibrates and thiazolidinediones (TZD). OK, MCT and LLC-PK1 cells were incubated for 12 h with the indicated drugs and concentrations, and aliquots of assay media were analyzed for LDH activity. Concentrations of agonists are shown as logarithmic units. The lethal mean concentration (LC_{50}) and the slope of the curves (Hill parameter) are indicated in the panels for WY14643 and ciglitazone. Fibrate panels (related to PPARα): squares are WY14643; triangles are clofibrate. TZD panels (related to PPARγ): squares are ciglitazone; triangles are pioglitazone.

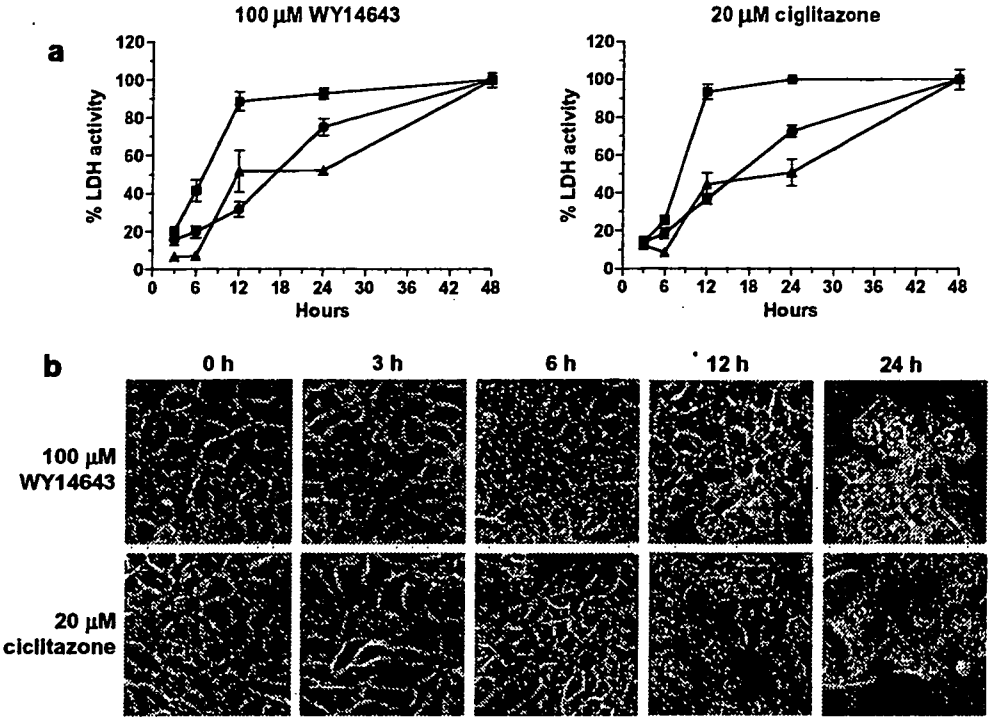

Fig. 2. Effect of WY14643 and ciglitazone as a function of time. (a) OK (squares), MCT (circles) and LLC-PK1 (triangles) cells were incubated with either 100 μM WY14643 or 20 μM ciglitazone at the indicated times, and LDH activity was assayed. (b) Phase-contrast pictures of LLC-PK1 cells incubated with WY14643 or ciglitazone at the indicated times.

increase, as shown with a Hill value of 13.9, and OK cells exhibited the lowest experimental concentration with a significant increase in LDH activity (5 μM ciglitazone).

3.2. Time dependence of PPAR agonist effects

Fixed PPAR ligand concentrations were used to analyze the course of their effects on cell viability. 100 μM WY14643 increased LDH activity in OK and MCT cells at 6 h of incubation, and it became a frank effect at 12 h in LLC-PK1 cells (Fig. 2a). Similar effects were obtained with 20 μM ciglitazone, which showed significant increases in LDH activity that were found at 6 h with OK and MCT cells and at 12 h with LLC-PK1 cells.

When combining dose–response relationships and time courses, different findings were observed: At 3 h of incubation, no cell death was detected at any of the concentrations of WY14643 or ciglitazone. However, at 6 h significant cytotoxicity was observed with 100 μM WY14643 and 20 μM ciglitazone. At 24 h toxicity was observed with 50 μM and 5 μM, respectively (data not shown).

A phase contrast optical inspection of the cells revealed a similar morphological process with either WY14643 or ciglitazone treatments. Fig. 2b shows the changes in LLC-PK1 cells, and identical alterations were seen with OK and MCT cells. The nucleoli of the cells become bright at just 3 h of treatment with both chemicals. This change is more pronounced at 6 h, when disorganization of the cytoplasm also starts to be observed. At 12 h the cells are separated and enlarged; some are already detached, and the cytosols are filled with vacuoles. All these modifications have greater intensity at 24 h. No evidence of chromatin condensation or clear hallmarks of apoptosis can be detected with this methodology. Finally, no changes with clofibrate or pioglitazone were observed at either concentration or incubation time in all three cell lines (data not shown).

3.3. Expression of PPARα and PPARγ in LLC-PK1 cells

The experiments designed to characterize the type of cell death induced by PPAR agonists were performed in LLC-PK1 cells. Therefore, the expression of the corresponding PPAR RNAs was determined by amplification of reverse transcribed cDNA by PCR. Fig. 3 shows that both PPARα and PPARγ RNAs are expressed with similar intensities in this cell line, i.e. a receptor-dependent mechanism of toxicity of PPAR agonists cannot be excluded.

3.4. WY14643 and ciglitazone disrupt stress fibers

Changes in morphology observed with phase contrast microscopy suggested alterations in cytoskeleton, and therefore we analyzed actin microfilaments in treated cells. LLC-PK1 cells were treated with 100 μM WY14643 and

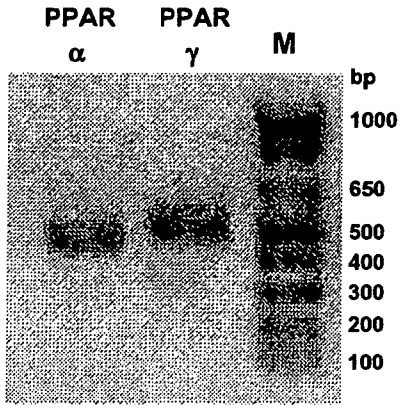

Fig. 3. RT-PCR of PPARα and PPARγ fragments. Both receptors are expressed with similar abundance in this cell line. M, marker with molecular sizes in base pairs.

10 μM ciglitazone, in both cases for 6 and 16 h, and stress fibers were stained with rhodamine-labeled phalloidin (Fig. 4). Modifications in polymerization were already evident at 6 h, but they were maximal at 16 h. Spaces between cells were already observed at 6 h, and clear alterations in cytoskeleton with extracellular debris were already at 16 h. However, no indications of apoptosis could be observed in these experiments.

3.5. Effects of WY14643 and ciglitazone on DNA intercalating dye staining

For a more in-depth analysis of the morphological changes produced by these two PPAR agonists, a double staining with acridine orange and ethidium bromide was performed. LLC-PK1 cells treated with either 100 μM WY14643 or 10 μM ciglitazone, for either 6 or 16 h, were stained as explained in Section 2 (Fig. 5). A differential interference contrast (DIC) analysis revealed a smooth pattern of confluent cells. Control cells showed a viable pattern of staining, including condensed nucleoli. Cells treated with either WY14643 or ciglitazone were stained in two patterns that were compatible with both viable cells (green cytoplasm and nuclei with orange dots as RNA) or necrotic cells (red cytoplasms and nuclei). The percentage of each pattern depended on the time, with most of the cells in the necrotic pattern at 16 h. A secondary necrosis (late apoptosis) was not evident under these conditions, because chromatin was not condensed. Cytosolic vacuoles were likewise very evident with the DIC optics.

3.6. Effect of WY14643 and ciglitazone on phosphatidylserine distribution

One of the earliest events in apoptosis involves the redistribution of phosphatidylserine from the inner to the outer layer of the plasma membrane. Therefore, to find out whether WY14643 and ciglitazone produced apoptosis as an early event or at low concentrations, we treated LLC-PK1 cells with two different concentrations and for two different times. To detect phosphatidylserine in apoptotic cells we used EGFP-annexin V (Martin et al., 1995). Control cells did not stain with either EGFP-annexin V or PI, and DIC optics evidenced a confluent mosaic of smooth LLC-PK1 cells (Fig. 6). In contrast, treatment with 50 μM WY14643 for 12 h altered the morphology of the cells as shown by the DIC, with an increase of vacuoles and many cells stained red with propidium iodide (PI).

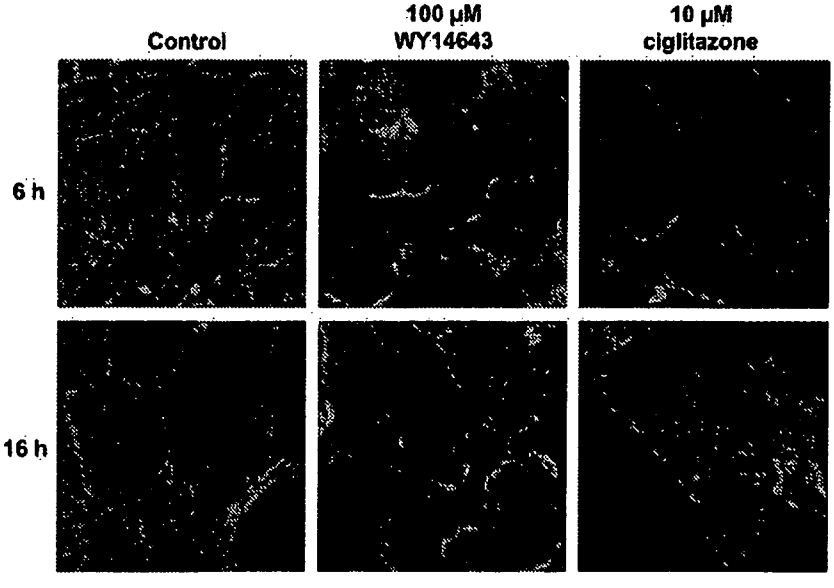

Fig. 4. Effect of WY14643 and ciglitazone on stress fibers. LLC-PK1 cells were incubated for 6 or 16 h with PPAR agonists, and then fixed and stained with rodhamine-conjugated phalloidin. At 16 h actin filaments have completely lost organization, and cellular shapes are modified, with separated bodies. After 6 h of incubation the effects on stress fibers are evident but of less intensity.